AD-A108 566 CALIFORNIA UNIV LOS ANGELES F/G 9/5
THEORETICAL AND EXPERIMENTAL INVESTIGATION OF SOME SLOT ANTENNA--ETC(U)
OCT 81 R S ELLIOTT, N G ALEXOPOULOS F19628-79-C-0069
UNCLASSIFIED RADC-TR-81-232 NL

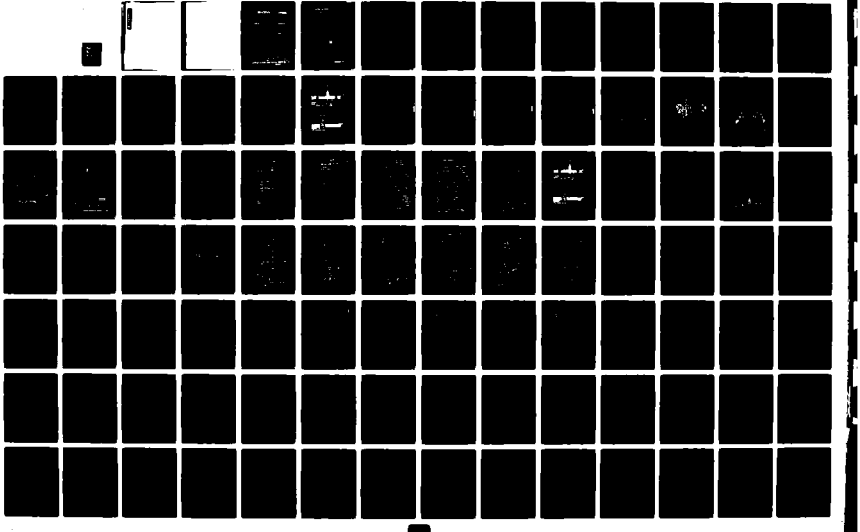

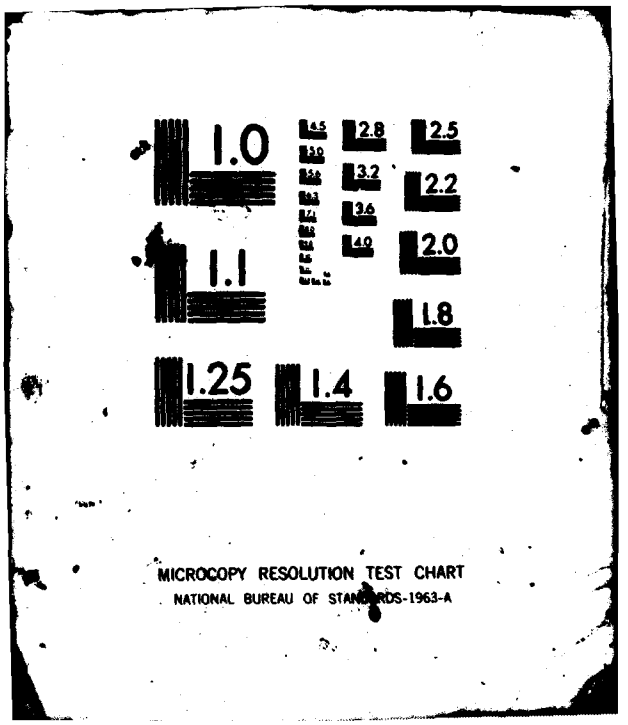
1.0
1.1
1.25
1.4
1.6
2.8
2.5
3.2
2.2
3.6
2.0
4.0
1.8
MICROCOPY RESOLUTION TEST CHART
NATIONAL BUREAU OF STANDARDS-1963-A

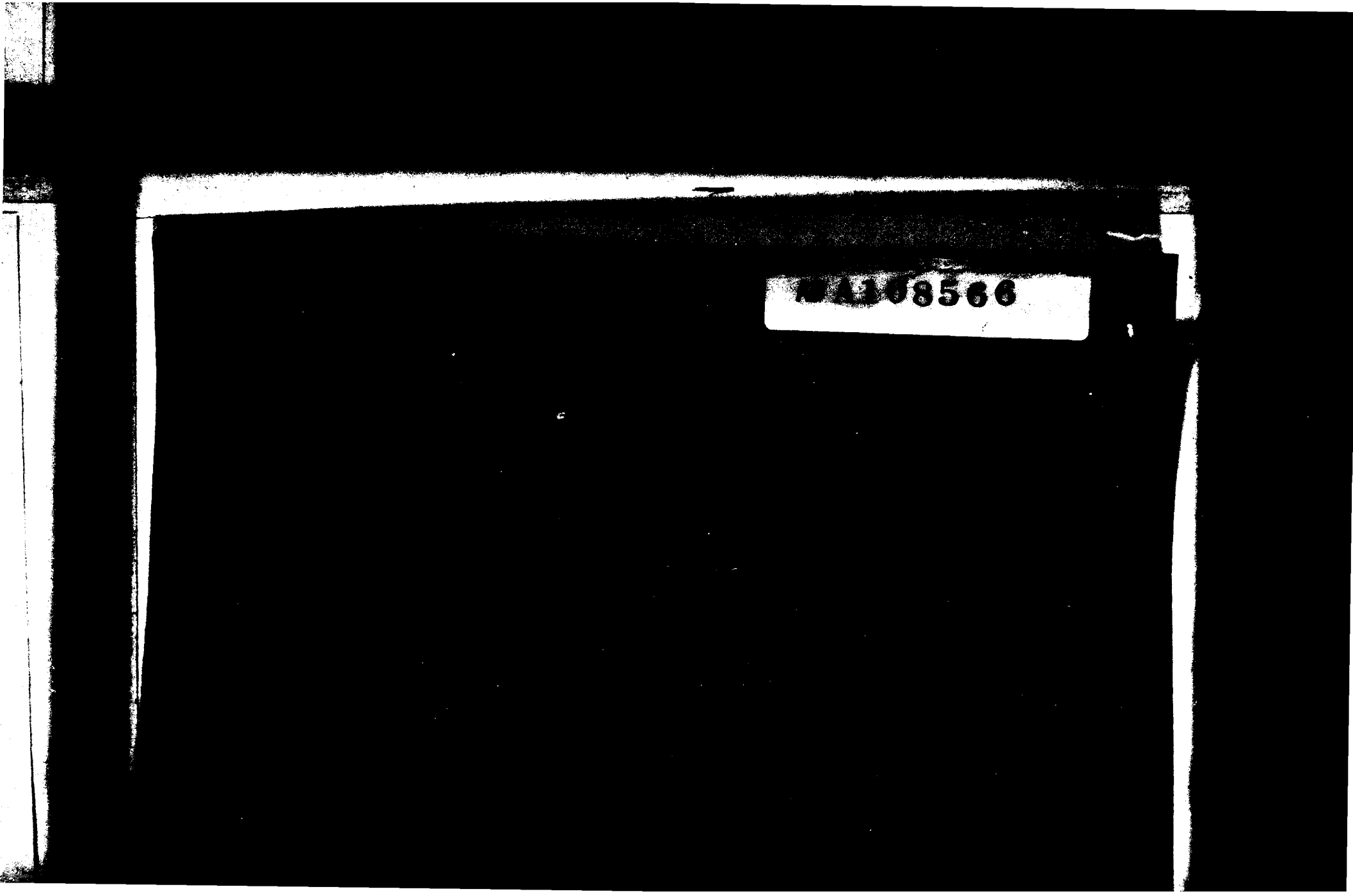
A368566

UNCLASSIFIED

SECURITY CLASSIFICATION OF THIS PAGE (When Data Entered)

REPORT DOCUMENTATION PAGE	READ INSTRUCTIONS BEFORE COMPLETING FORM
1. REPORT NUMBER: RADC-TR-81-232	2. GOVT ACCESSION NO: AD-A108566	3. RECIPIENT'S CATALOG NUMBER
4. TITLE (and Subtitle): THEORETICAL AND EXPERIMENTAL INVESTIGATION OF SOME SLOT ANTENNA ARRAY PROBLEMS	5. TYPE OF REPORT & PERIOD COVERED: Final Technical Report 1 Feb 79 - 7 Mar 81
	6. PERFORMING ORG. REPORT NUMBER: N/A
7. AUTHOR(s): R.S. Elliott, P.J. Contoyannis, N.G. Alexopoulos, P. Park, G. Franceschetti	8. CONTRACT OR GRANT NUMBER(s): F19628-79-C-0069
9. PERFORMING ORGANIZATION NAME AND ADDRESS: University of California, Los Angeles CA 90024	10. PROGRAM ELEMENT, PROJECT, TASK AREA & WORK UNIT NUMBERS: 61102F, 2305J327
11. CONTROLLING OFFICE NAME AND ADDRESS: Deputy for Electronic Technology (RADC/EEA), Hanscom AFB MA 01731	12. REPORT DATE: October 1981
	13. NUMBER OF PAGES: 116
14. MONITORING AGENCY NAME & ADDRESS (if different from Controlling Office): Same	15. SECURITY CLASS. (of this report): UNCLASSIFIED
	15a. DECLASSIFICATION/DOWNGRADING SCHEDULE: N/A

16. DISTRIBUTION STATEMENT (of this Report)

Approved for public release; distribution unlimited.

17. DISTRIBUTION STATEMENT (of the abstract entered in Block 20, if different from Report)

Same

18. SUPPLEMENTARY NOTES

RADC Project Engineer: Nicholas P. Kernweis (EEA)

19. KEY WORDS (Continue on reverse side if necessary and identify by block number)

Slot Array Antenna
Slot Coupling with Intersticed Baffles
Strip Line Fed Slots

20. ABSTRACT (Continue on reverse side if necessary and identify by block number)

The effect of metallic fences on mutual coupling between slots of a slot antenna is studied. A model solution has been obtained whereby the fence is modelled as a thin half elliptic cylinder. This model allows for thickness to be taken into account and provides exact relations for mutual impedance computations. The geometrical theory of diffraction has been adopted to analyze an antenna array when the [illegible] are not too close to the fences. [illegible]

DD FORM 1473 EDITION OF 1 NOV 65 IS OBSOLETE

SECURITY CLASSIFICATION OF THIS PAGE (When Data Entered)

072250

transverse stripline-fed slots have been developed. A design procedure for such slot arrays requires knowledge of the mutual coupling relation as well as the self-impedance properties of a slot. Preliminary design equations are reported in this document.

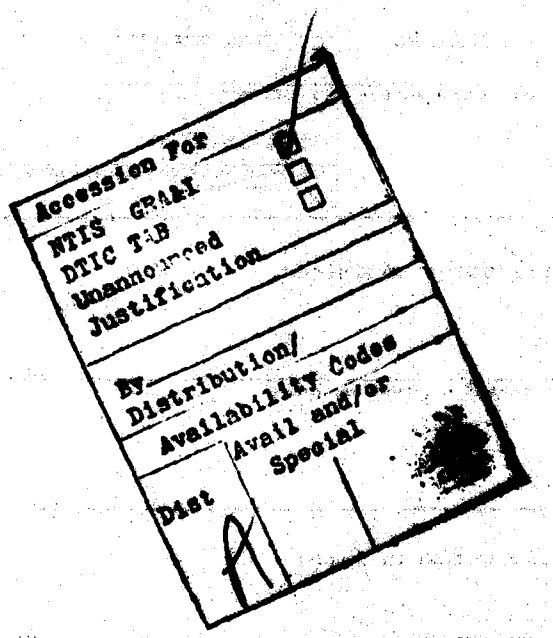

TABLE OF CONTENTS

INTRODUCTION

The effect of metallic fences on mutual coupling between slot antennas is studied. A model solution has been obtained whereby the fence is modelled as a thin half elliptic cylinder. This model allows for thickness to be taken into account and provides exact solutions to mutual impedance computations. In addition, the geometrical theory of diffraction has been adopted to analyze an exceedingly thin fence, when the slot antennas are not too close to the fence.

In addition design procedures for longitudinal and transverse stripline-fed slots have been developed. A design procedure for such slot arrays requires knowledge of the mutual coupling relation as well as the self-impedance properties of a slot. Preliminary design equations are reported in this document.

1. Coupling Between Slot Antennas With a Baffle In Between.

In the effort to influence mutual coupling between slot antennas in a desirable way the following problem has been considered: A septum or baffle has been placed between two infinite slot antennas. In order to provide an extra degree of freedom the septum has been assumed to be a half elliptic cylinder as shown in Figure 1.1. In this manner not only thickness is included in the computation but, more important, the problem becomes amenable to an exact modal solution. Using the model depicted in Figures 1.1 and 1.2, one can obtain an exact expression for the mutual admittance, realizing that the equivalent problem is that of scattering by a magnetic line source from an electrically perfect conducting elliptic cylinder. The solution is obtained in terms of Mathieu functions [1.1] and is given by

$$Y_{21} = \frac{-k}{2\eta} H_o^{(1)}[k(d_1 + d_2)] - 4 \sum_{xx=\begin{cases} AE \\ BD \end{cases}} \sum_n \frac{T_{xx_n}\left(\frac{\pi}{2}\right) T_{xx_n}\left(-\frac{\pi}{2}\right)}{N_n^{xx}(9)} \cdot$$

$$\cdot \frac{T'_{xx_n}(u_s)}{N_n'^{(1)}(u_s)} R^{(1)}_{xx_n}(u_s) R^{(1)}_{xx_n}(u) \qquad (1.1)$$

where $T_{xx_n}(u)$ and $R^{(1)}_{xx_n}(u)$ are the angular and radial solutions to the Mathieu equation respectively. The $N_n^{xx}(9)$ are normalizing factors.

Typical dependence of the magnitude of the mutual admittance on the slot separation for various values of the height and the thickness of the septum is depicted in Figures 1.3, 1.4. Each Figure contains the curves corresponding to one height of the septum, so that the effect of the

septum thickness can be determined. Figures 1.5, 1.6 contain the same curves but rearranged so that each figure displays curves corresponding to the same thickness of the septum, so that the effect of the height can be displayed.

Although the results discussed up to this point are exact, the modal series solution converges very slowly as the septum height-to-thickness ratio increases and/or the separation between slots increases. In order to circumvent this difficulty, a different approach has been adopted to solve the problem for these limiting cases. The approach is based on the geometrical theory of diffraction. In this approach, the equivalent problem of diffraction by a strip is transformed to another equivalent problem, namely that of diffraction by a slit. [1.2] If the interactions between edges are neglected, the mutual admittance is obtained in the form

$$Y_{21} = -\frac{\exp[-jk(R_1+R_2)]}{2\pi k\sqrt{R_1R_2}}\left[\frac{T(\xi^+)}{\cos\left(\frac{\phi_1+\phi_2}{2}\right)} + \frac{T(\xi^-)}{\cos\left(\frac{\phi_1+\phi_2}{2}\right)}\right] \tag{1.2}$$

where

$$\xi^{\pm} = \sqrt{2k\frac{R_1R_2}{R_1+R_2}}\cos\left(\frac{\phi_1\pm\phi_2}{2}\right), \tag{1.3}$$

$$T(\xi) = 2j\xi\exp(j\xi^2)\int_{\xi}^{\infty}\exp(-jt^2)dt \tag{1.4}$$

and R_1, R_2 are the distances to the tip of the septum from the slots. Results based on (1.2) have been computed and presented in Figures 1.3-1.6 for comparison with the exact modal solution. The agreement shown in these curves is very good, especially as the separation between antennas and/or

the septum height-to-septum-thickness ratio increases. More refined GTD computations have also been carried in which the infinite ray interactions between the slit edges have been taken into account [1.2]. The additional contribution to Y_{21} is

$$\Delta Y_{21} = \frac{2}{\eta k \sqrt{R_1 R_2}} \exp\left[-jk(R_1+R_2)\right] T(\sqrt{2ka})$$

$$\frac{\sqrt{\frac{1}{\pi ka}} \exp(-2jka) \exp(-j\frac{\pi}{4}) T(\sqrt{2ka})}{1 + \sqrt{\frac{1}{\pi ka}} \exp(-2jka) \exp(-j\frac{\pi}{4}) T(\sqrt{2ka})} \qquad (1.5)$$

Further refinements have also been achieved by considering a spectral approach to include the curvature of the cylindrical diffracted waves [1.2]. Numerical computations which include these refinements are being undertaken presently and the results will ultimately be included in a journal paper.

References [1.1] and [1.2] are attached to this Final Report as Appendices A and B.

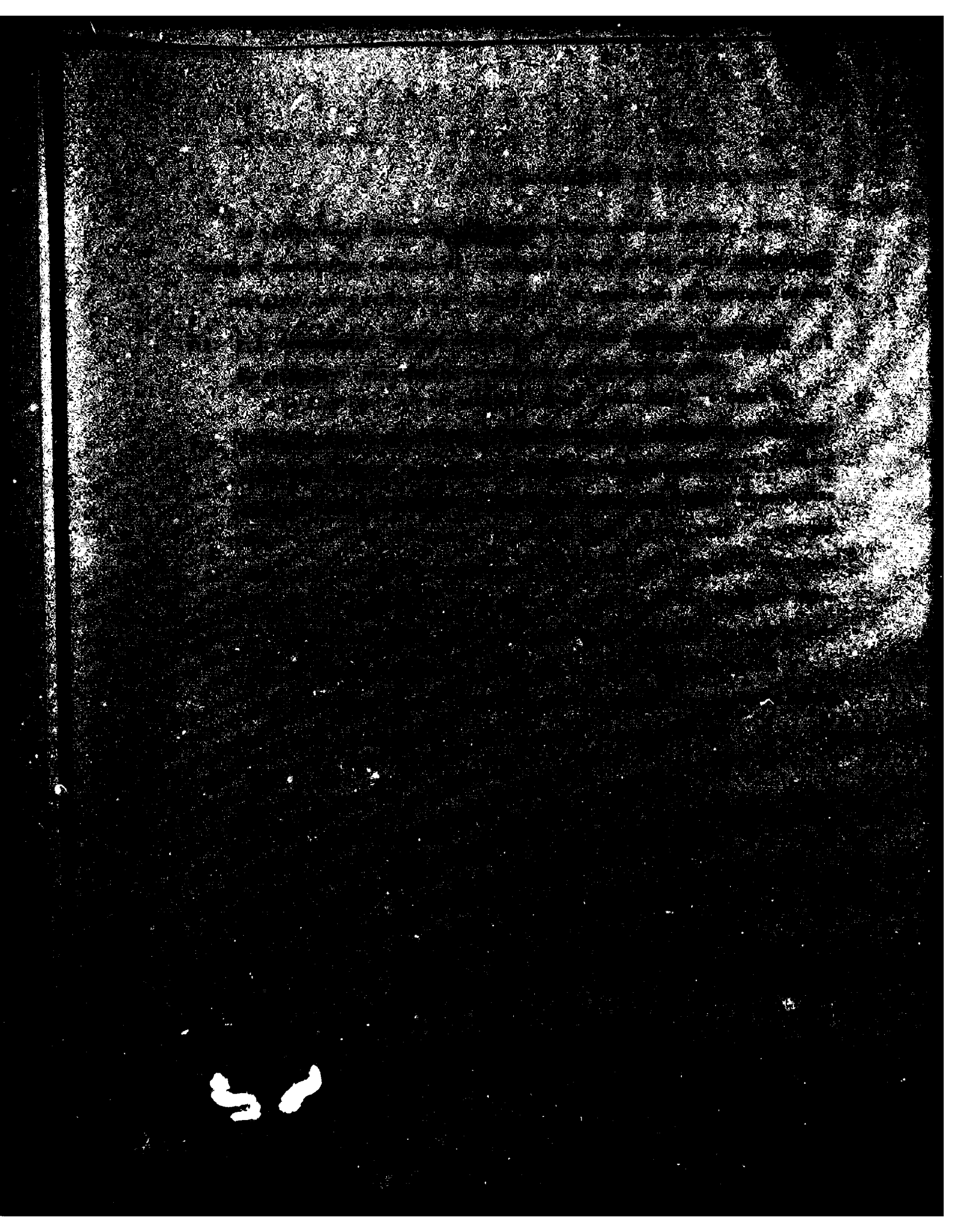

2. Design Procedure for Stripline-Fed Slots.

Here, a study has been made and has been completed successfully of longitudinal slots fed by boxed stripline. In addition significant progress can be reported on the design of transverse slots fed by boxed stripline.

2.1 Longitudinal Slots

An array of longitudinal slots, centered on the broad wall of a rectangular waveguide, will not radiate if excitation is by a TE_{10} mode. However, if the waveguide is converted to a boxed stripline, with the strip meandering under the slots as shown in Figure 2.1, slot excitation can occur. The electric field induced in a particular slot has a complex amplitude which is a function of 1) the angle at which the strip passes under the slot, and 2) the length of the slot. Additional contributions to the electric field in the slot occur if other slots are present.

A design procedure for such slot arrays requires knowledge of the mutual coupling relation as well as the self-impedance properties of a slot [2.1]. The key equations of the pertinent analysis are [2.1]:

$$I_n = \frac{2f_n(\theta_n,\ell_n)}{Z_n^a} V_n^s \tag{2.1}$$

$$Z_n^a = \frac{4|f_n(\theta_n,\ell_n)|^2}{\frac{4|f_n(\theta_n,\ell_n)|^2}{Z_n} + \sum_{m=1}^{N}{}' \frac{V_m^{s*}}{V_n^{s*}} Y_{nm}^{2w*}} \tag{2.2}$$

in which $f(\theta,\ell)$ is a known function of the slot half-length ℓ and the strip tilt θ, found through interaction of the TEM with an assumed cosinusoidal field distribution in the slot. I_n is the mode current, common to all array elements in a standing wave array, Z_n^a is the active impedance of the n^{th} slot, Z_n is its self impedance, and V_n^s is the slot voltage distribution. Y_{nm}^{2w} is the mutual admittance between slots in an equivalent slot array that is two-wire fed.

One uses these equations in an actual design by first accumulating experimental data on a single slot to obtain the self impedance function $Z_n(\theta_n,\ell_n)$. This function is a polyfit to the measured data, an example being given in Figure 2.2. With $f_n(\theta_n,\ell_n)$ and $Z_n(\theta_n,\ell_n)$ stored in the computer, a computation can be made of

$$Y_n^b = \sum_{m=1}^{N}{}' \frac{V_m^{s*}}{V_n^{s*}} Y_{nm}^{2w*} \tag{2.3}$$

using the known desired slot voltage distribution (known because the pattern is specified), with values for Y_{nm}^* calculated using assumed starting lengths for the slots.

The computer then searches for a (θ_n,ℓ_n) combination which satisfies

$$\mathrm{Im}\,\frac{4|f_n(\theta_n,\ell_n)|^2}{Z_n(\theta_n,\ell_n)} = -\,\mathrm{Im}\,Y_n^b \tag{2.4}$$

for this will make Z_n^a pure real, as can be seen from equation (2.2).

It turns out that there is a continuous sequence of couplets (θ_n,ℓ_n) which will satisfy (2.4). Which one to choose is a question to which we shall return shortly. But for the moment, let us select one of these couplets and store it, going on similarly to find a continuous sequence of

couplets (θ_m, ℓ_m) which will satisfy (2.4) for the n^{th} slot. Only one member of this sequence will pair properly with the chosen couplet (θ_n, ℓ_n), because we must also satisfy

$$\frac{I_m}{I_n} = \frac{f_m(\theta_m, \ell_m)}{f_n(\theta_n, \ell_n)} \frac{z_n^a}{z_m^a} \frac{V_m^a}{V_n^a} \tag{2.5}$$

as can be seen from equation (2.1). Thus, for the chosen (θ_n, ℓ_n), we get a set of companion couplets (θ_1, ℓ_1), (θ_2, ℓ_2), $\ldots\ldots(\theta_N, \ell_N)$.

Did we store the right couplet $(\theta_n \ell_n)$? This depends on the desired input impedance,

$$z_m = \sum_{n=1}^{N} z_n^A \tag{2.6}$$

If the sum of the z_n^a terms is too low (high), a greater (lesser) tilt θ_n should have been chosen. This correction can be made in the next iteration, which must be undertaken anyway, because now improved values of Y_{nm}^{2w} can be computed, since the ℓ_n values have been updated. One keeps iterating until the couplets (θ_1, ℓ_1), etc. have settled down to values which deviate less than the attainable mechanical tolerances.

This procedure was used to design a 1 by 10 and a 2 by 10 array, with the dimensions given in Reference 2.1. A uniform slot excitation was specified. Only the 1×10 array was built, for which Z_{in}/Z_o was specified to be 2.0. The theoretical and experimental H plane patterns are displayed in Figure 2.3 and are seen to be in good agreement. The measured normalised input impedance was 1.8. There was a down-shift in center frequency of 3% due to a mis-selection of dielectric constant (2.55 instead of 2.45) but overall the performance was very good, and one can say with confidence that the theory and design were validated.

A contribution of considerable importance, in addition to the design procedure itself, was the idea to place the slots on the centerline. This achieved two beneficial results: 1) scattering in the TE_{10} mode was eliminated, permitting a wider box, shorter resonant slots, and thus practical slot spacings, and 2) the elimination of a cross-polarized pattern and the risk of grating lobes [2.2], [2.3].

2.2. Transverse Slots

The longitudinal slot arrays described above are suitable for use in applications where the desired polarization should be transverse to the boxed stripline, and the beam is not scanned too close to endfire. The other polarization has its applications too, and has the virtue of an element pattern which does not preclude scanning close to endfire. Thus it seemed desirable to extend the investigation to the case of transverse slots fed by boxed stripline.

The coupling to such slots is so inherently strong that the strip must be offset so as to pass under the slot near one of its extremities, as suggested in Figure 2.4. That reasonable self impedance data can be obtained with this configuration is evidenced by the measured data shown in Figure 2.5.

The theory parallels what was done for longitudinal slots and results in a pair of design equations identical in form to (2.1) and (2.2), with $f_n(\theta_n, \lambda_n)$ replaced by $f_n(s_n, \lambda_n)$, wherein s_n is the transverse offset of the strip from the center of the slot. The function $f_n(s_n, \lambda_n)$ is derived theoretically from an integration involving the TEM mode and the assumed electric field distribution in the slot [2.4].

The form we obtained for $f_n(s_n,t_n)$ was based on the assumption that there was a cosinusoidal standing wave electric field distribution in the slot. This is a reasonable assumption in the longitudinal case, with the strip crossing under the center of the slot. But is it a good assumption in the transverse case, with the strip crossing under the slot extremity? We were not confident about this assumption, and decided to test it by computing the back scattering for a resonant slot, to see if we got results consistent with data extracted from Figure 2.5.

Agreement was reasonable, as can be seen from the curves in Figure 4.6, but still there was a disagreement of about 20%. Was this serious enough to give an unsatisfactory array design? We could not tell, but since building an array is a costly and time-consuming process, we decided first to try to improve on our estimation of the electric field distribution in the slot.

A brute force approach would be to match tangential $\underline{H}$ across the slot and use the method of moments to calculate E_{slot}. But this requires knowledge of the complete Green's function for boxed stripline. The individual modes cannot be expressed as simple functions; indeed, we expended considerable effort just to get the functional form of the TEM mode. Thus this approach seemed prohibitively costly and has not been attempted.

We did try several obvious approaches, described in R & D Status Reports 5 and 6. These included a one-term Fourier series for the slot field distribution, a model based on an equivalent dipole, and an attempt to explain the 20% discrepancy as being due to the presence of the pins. None of these approaches has served to eliminate or even explain the discrepancy. In some frustration, we decided to go ahead and design an eight element

array, based on the cosinusoidal field assumption, specifying uniform excitation and an input match. We should learn a lot from testing this array. If agreement with prediction is poor, we will know the 20% discrepancy is serious. We can 'tune' this array by using a razor blade and conducting tape to shift the slots and alter their length. By cut and try this should ultimately produce a decent pattern and input impedance. We can then see by how much the slot dimensions had to be altered and gain a measure of the tolerances required.

REFERENCES

2.1 Pyong K. Park, "Theory, Analysis and Design of a New Type of Strip Fed Slot Array," Ph.D. Dissertation, University of California, Los Angeles, 1979.

2.2 P.K. Park and R.S. Elliott, "Design of Collinear Longitudinal Slot Arrays Fed by Boxed Stripline." Presented at the AP/URSI International Symposium, Quebec, Canada, June, 1980.

2.3 P.K. Park and R.S. Elliott, "Longitudinal Slot Arrays Fed by Boxed Stripline," IEEE Transactions, Antennas and Propagation, vol. AP-29, No. 1, pp. 135-140; January 1981.

2.4 P.K. Park and R.S. Elliott, "Design of Transverse Slot Arrays Fed by Boxed Stripline." Presented at the University of Illinois Allerton Symposium, September, 1980.

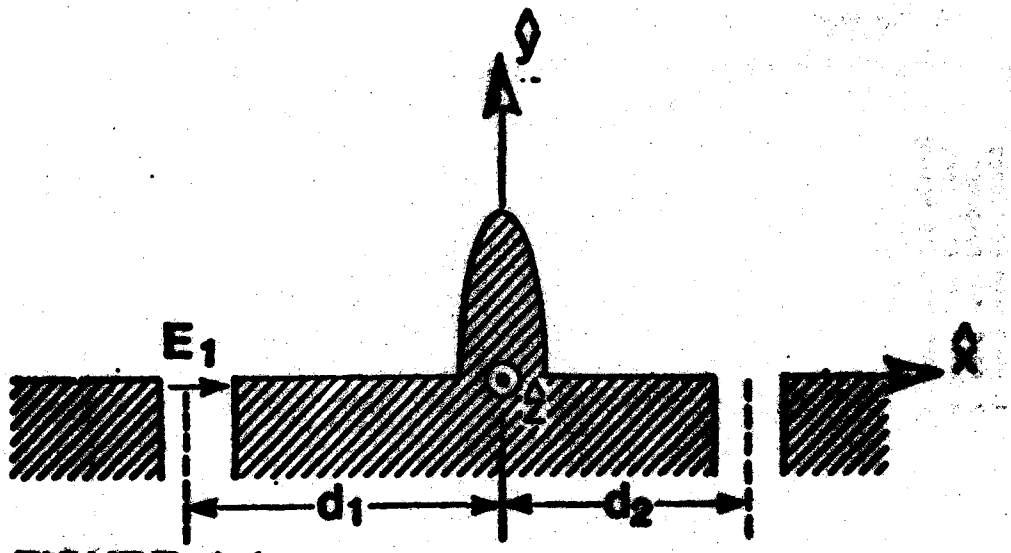

FIGURE 1.1
Model of the two slots separated by a metalic fence problem.

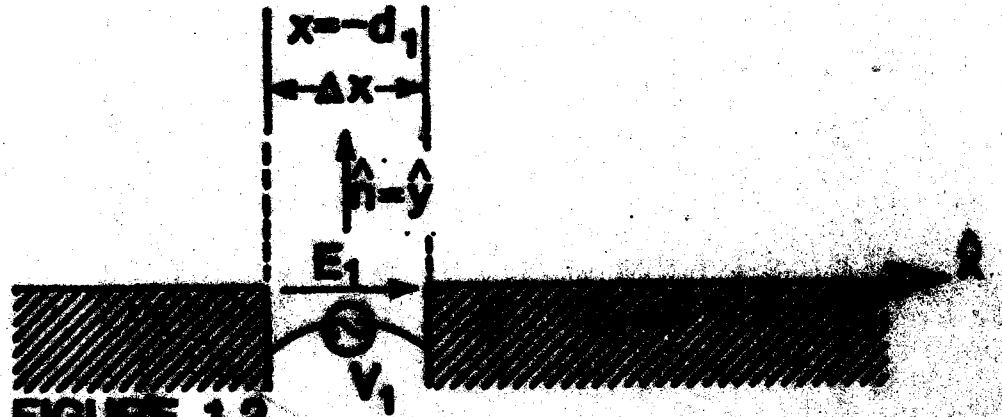

FIGURE 1.2
The radiating slot.

ADMITTANCE

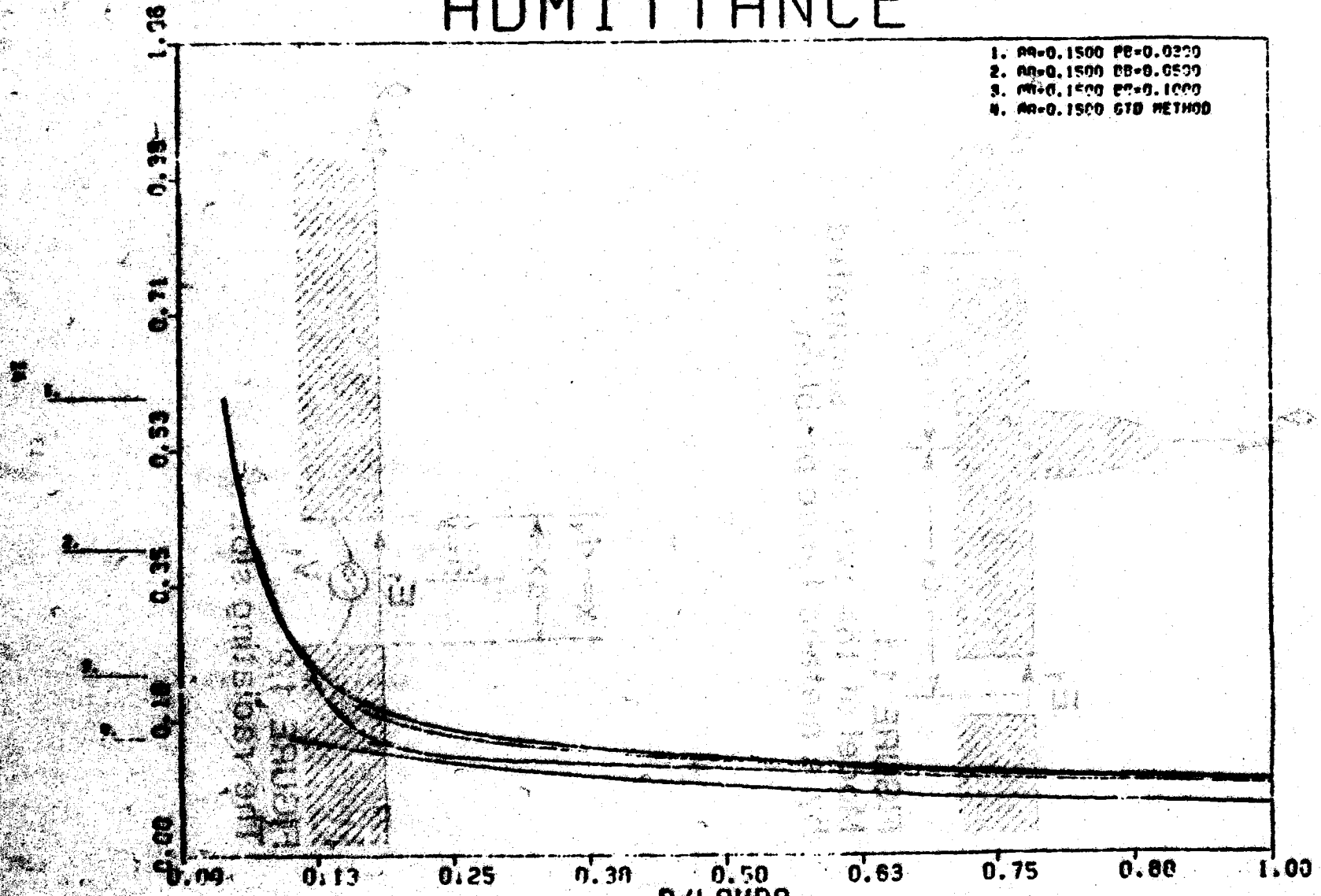

FIGURE 1.3

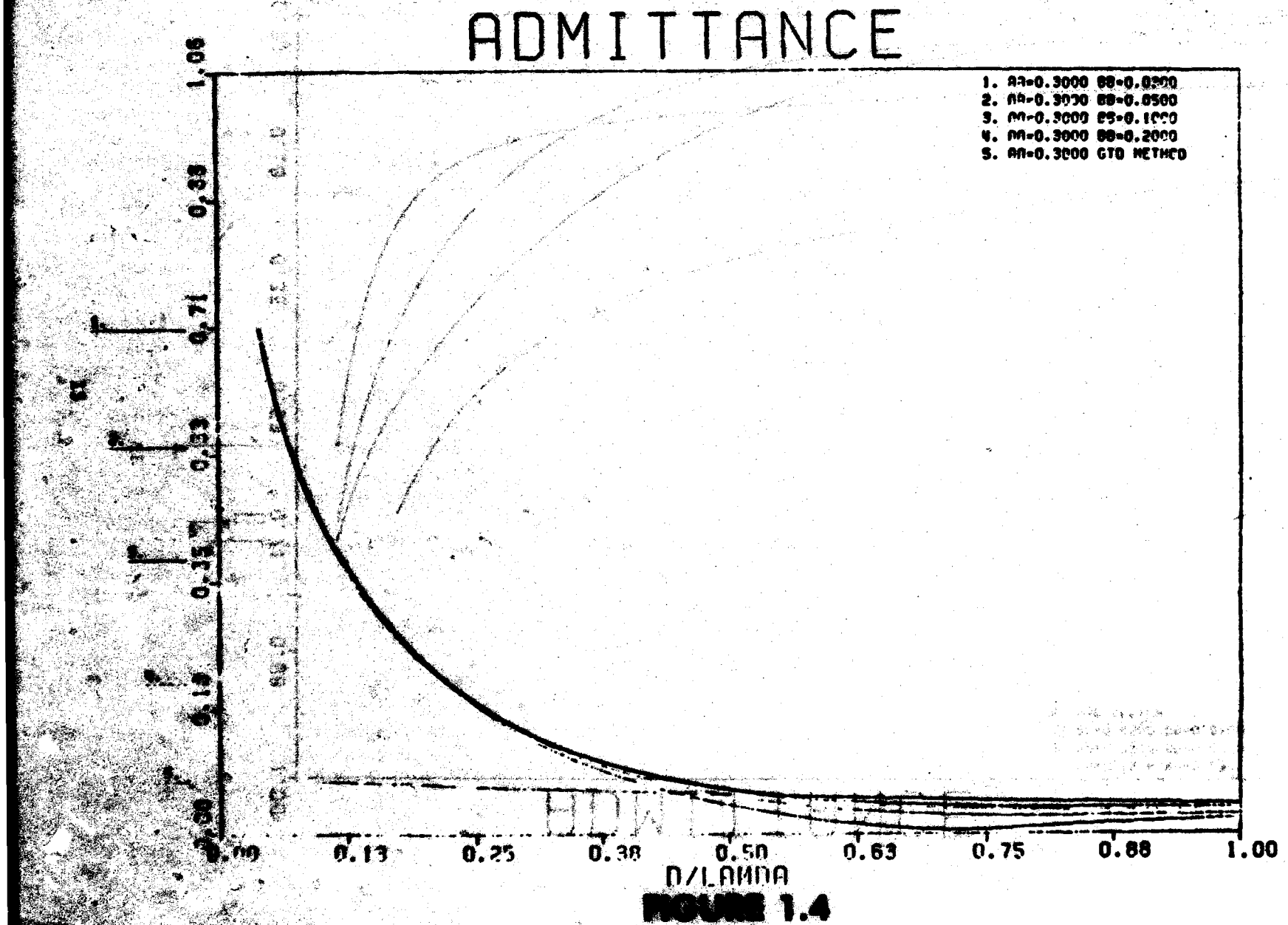
ADMITTANCE
1. AA=0.3000 BB=0.0300
2. AA=0.3000 BB=0.0500
3. AA=0.3000 BB=0.1000
4. AA=0.3000 BB=0.2000
5. AA=0.3000 GTD METHOD
1.00
0.88
0.75
0.63
0.50
0.38
0.25
0.13
0.00
D/LAMDA

FIGURE 1.4

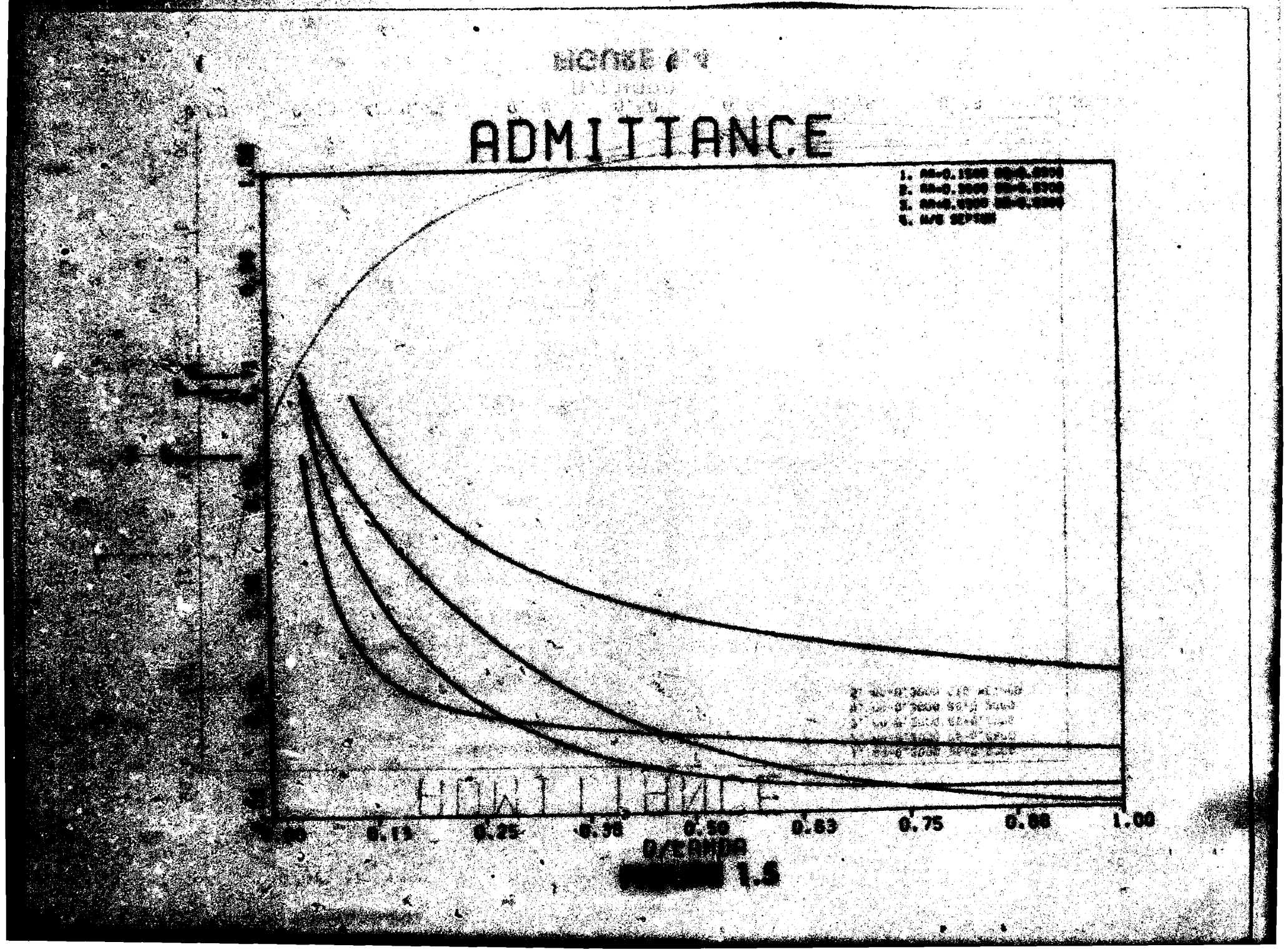
ADMITTANCE
0.13
0.25
0.50
0.63
0.75
1.00

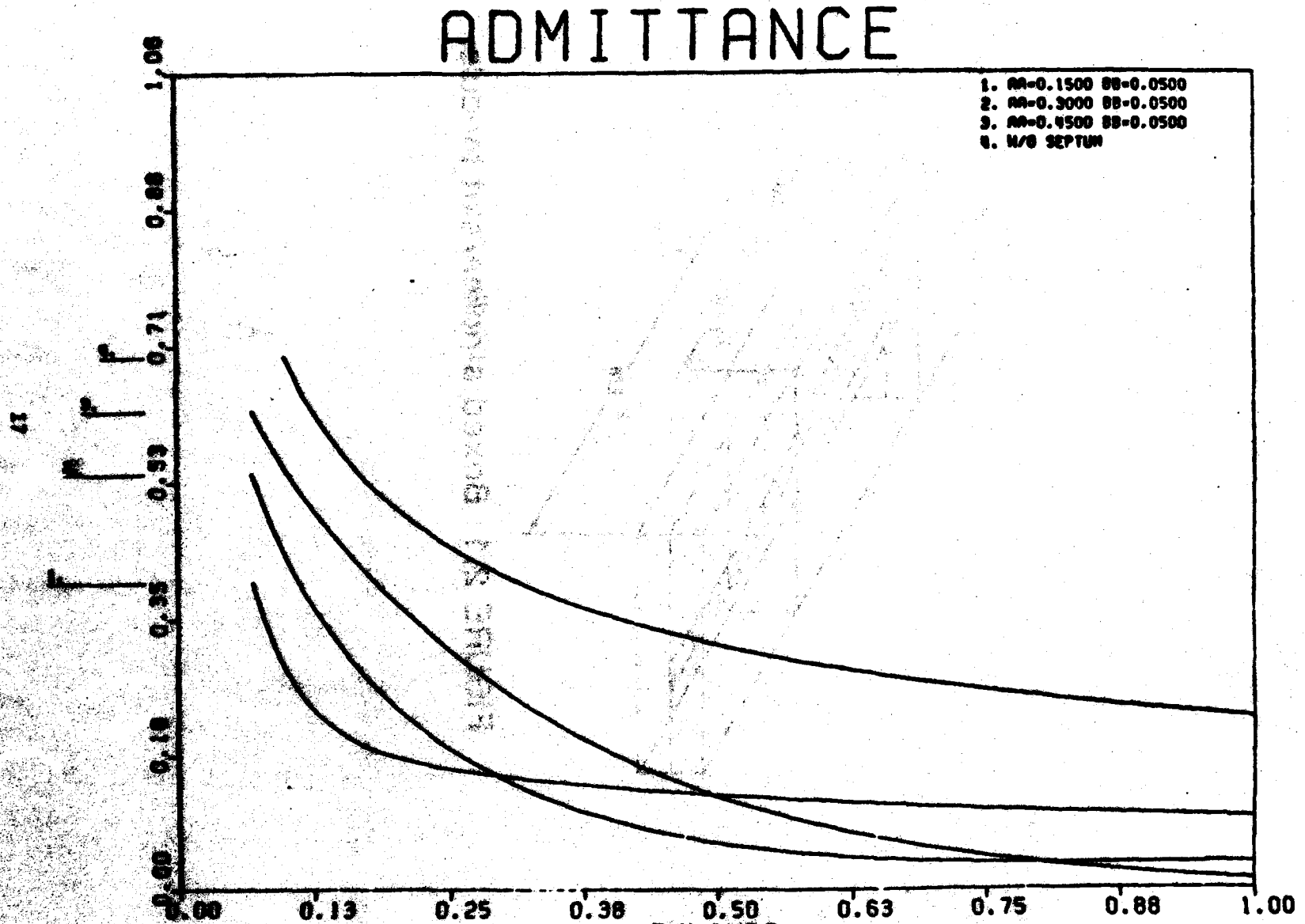
ADMITTANCE
1. AA=0.1500 BB=0.0500
2. AA=0.3000 BB=0.0500
3. AA=0.4500 BB=0.0500
4. H/G SEPTUM
1.00
0.88
0.75
0.63
0.50
0.38
0.25
0.13
0.00
D/LAMDA

FIGURE 1.6

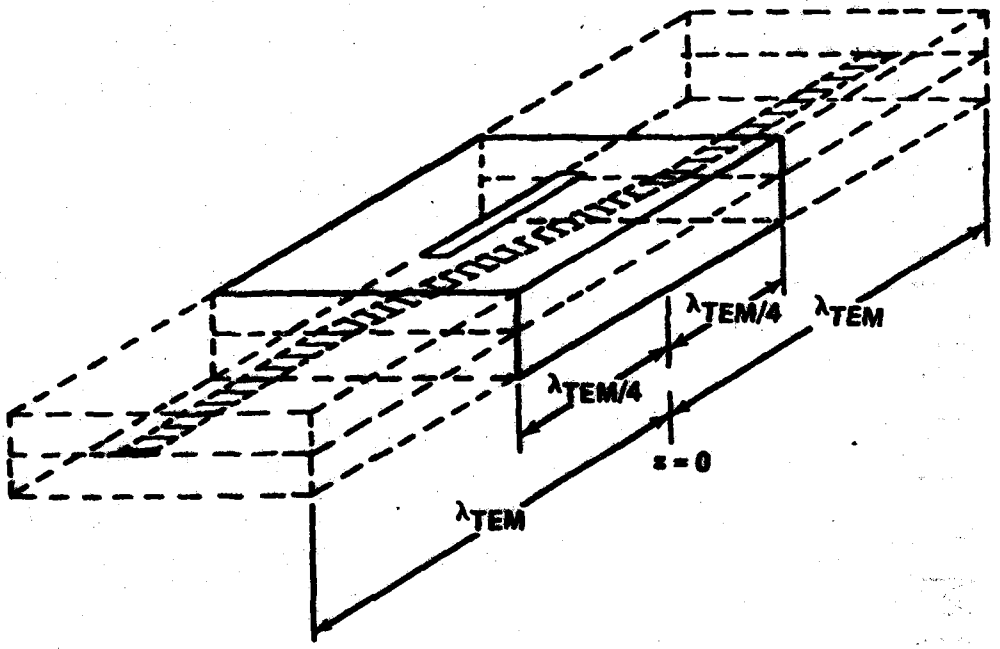

FIGURE 2.1 Boxed stripline/slot module.

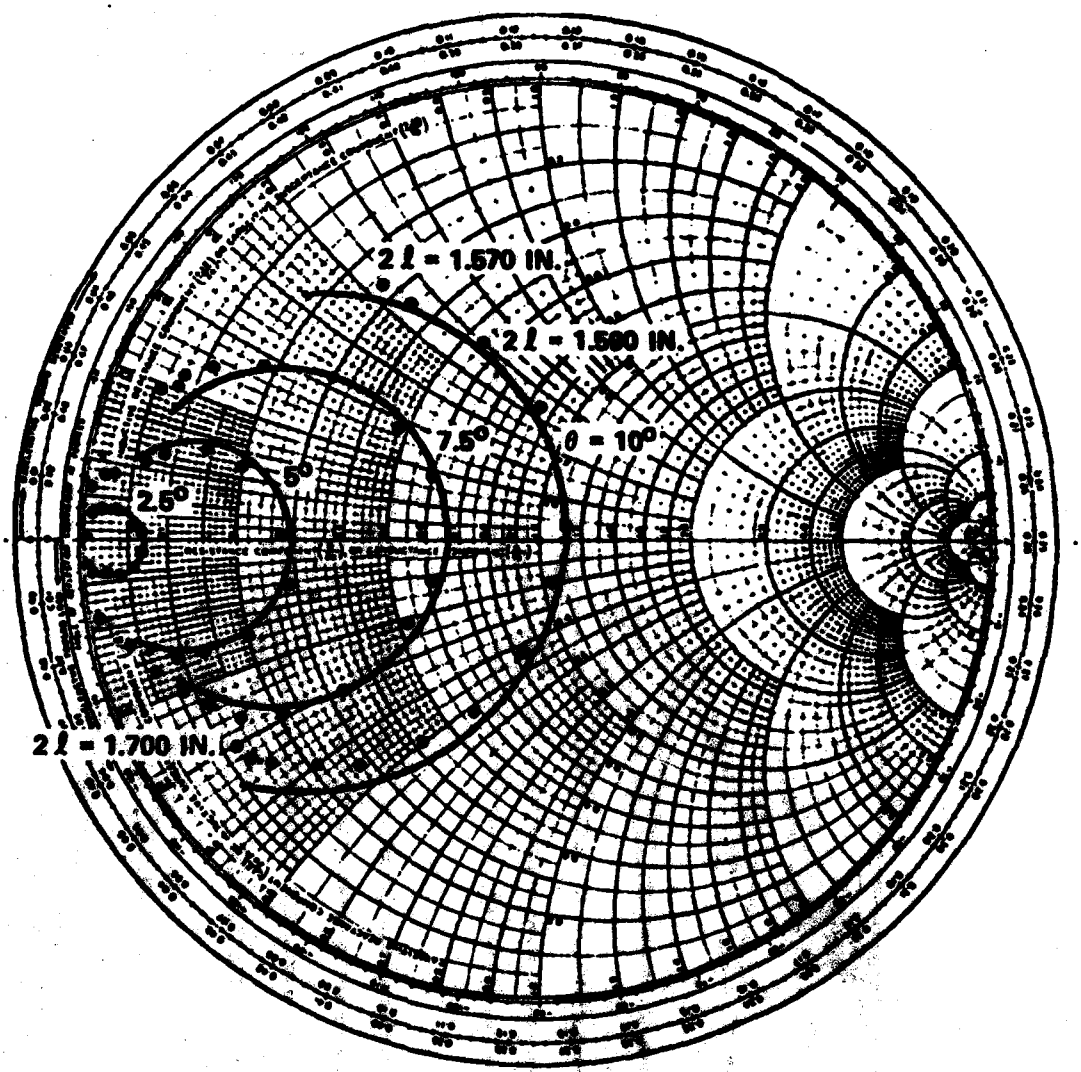

FIGURE 2.2 Slot self-impedance on Smith Chart.

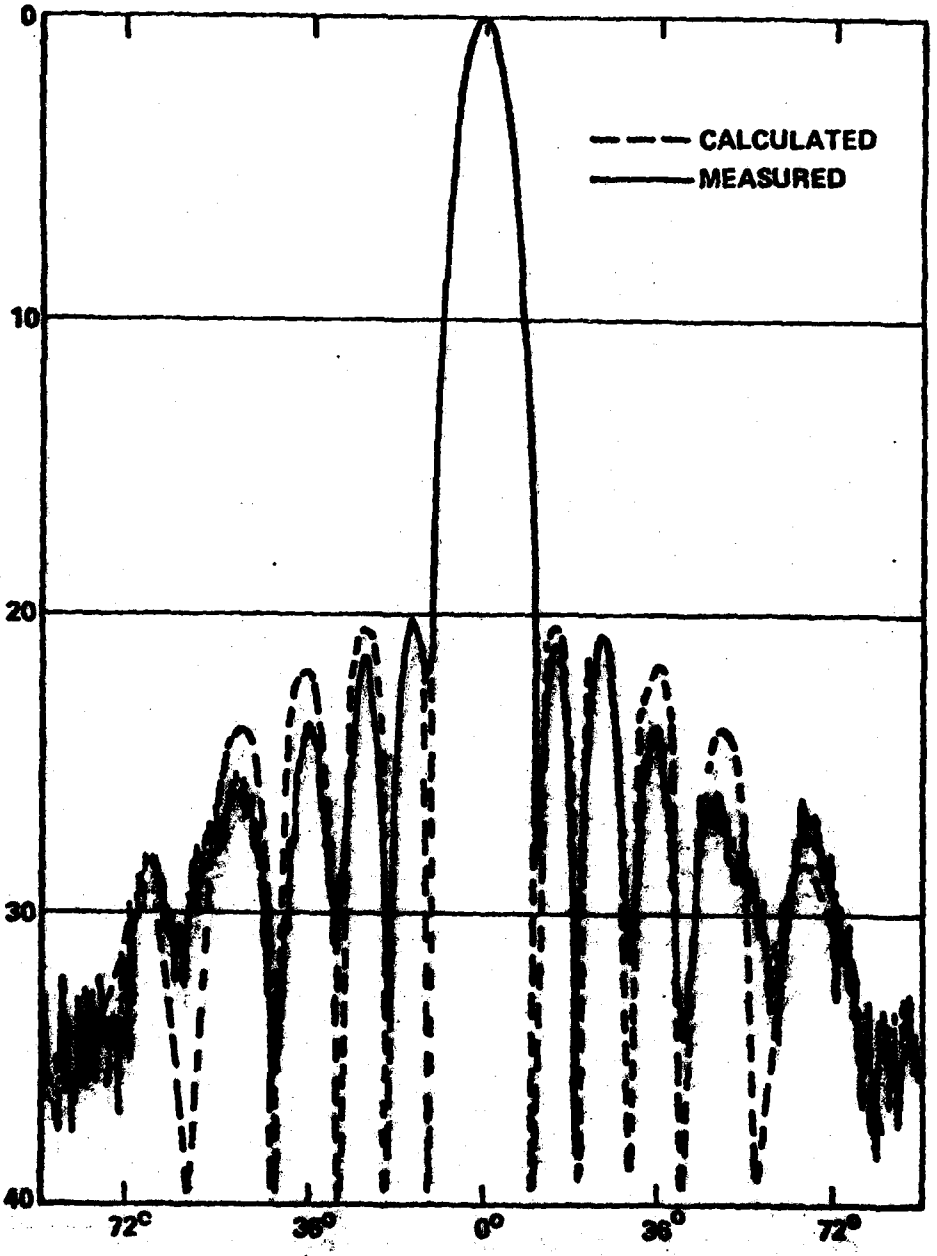

FIGURE 2.3 Caculated and measured patterns for the 20 dB Chebyshev Array at 2.42 Ghz.

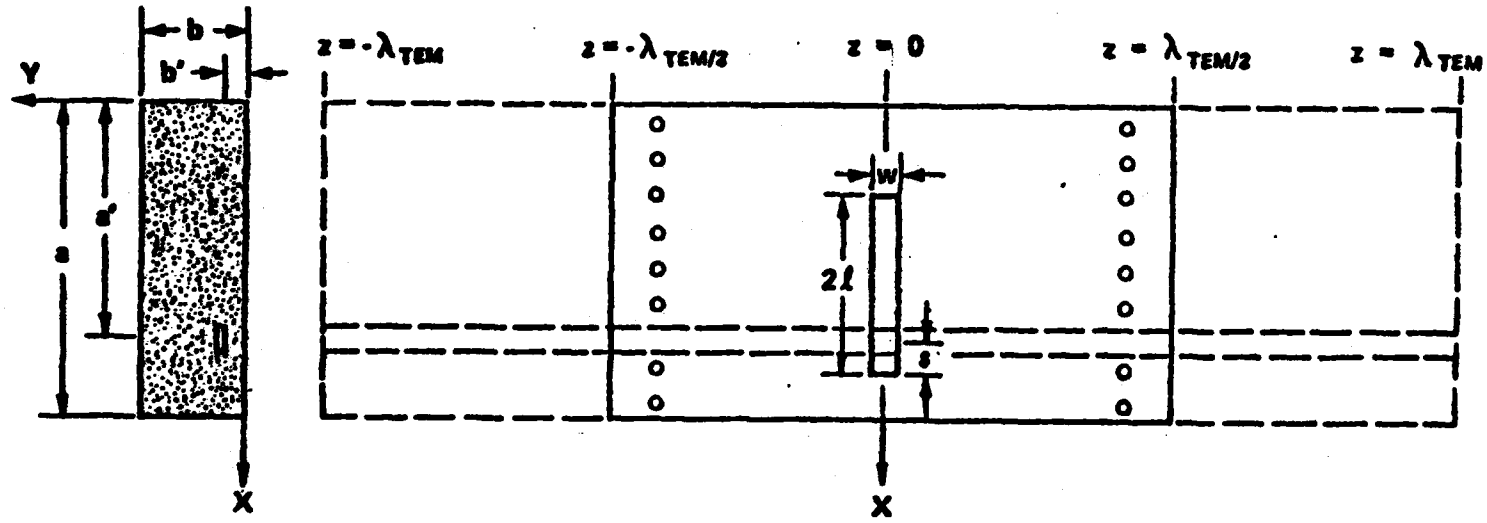

FIGURE 2.4 Extended Transverse Slot Module

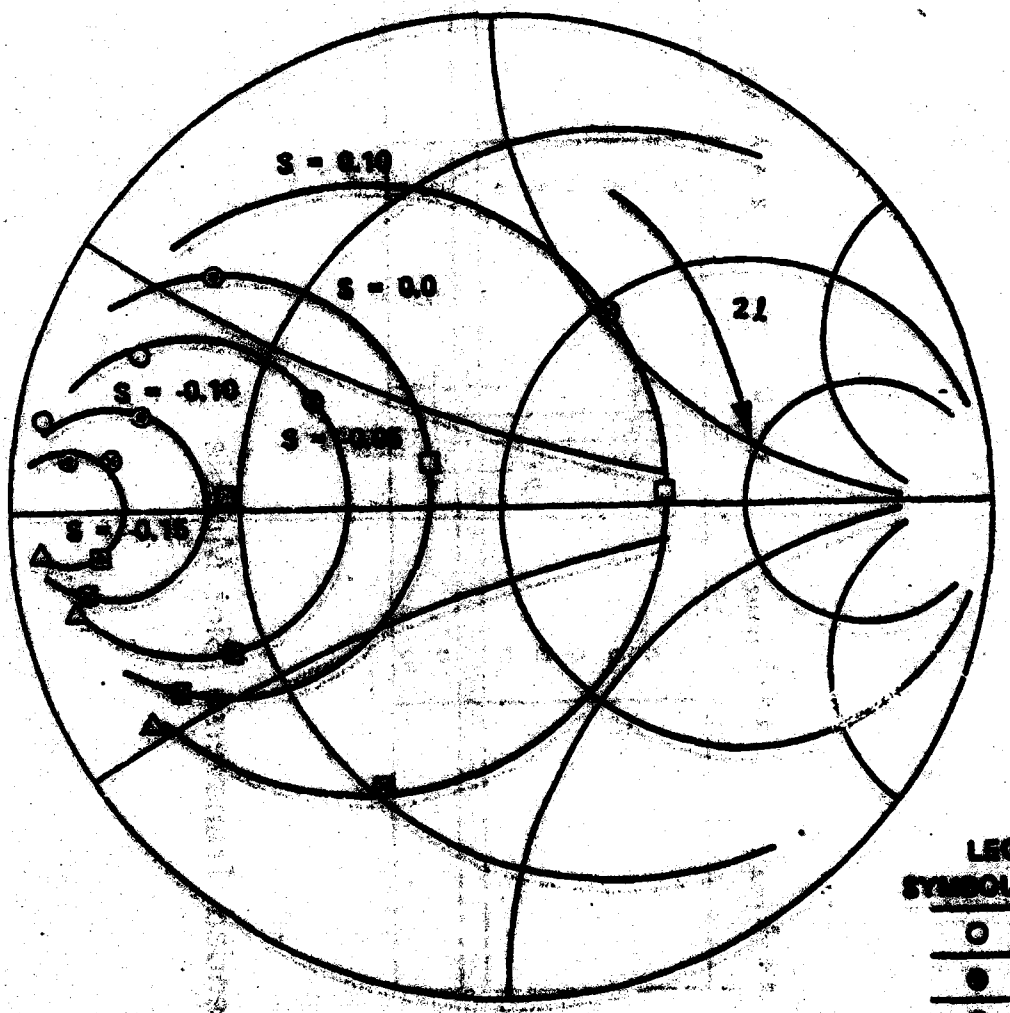

LEGEND	
SYMBOL	2.1
○	1.85"
●	1.9"
◉	1.95"
□	2"
■	2.05"
▣	2.1"
△	2.15"

FIGURE 2.5 Self-impedance data for single probe. f = 1.75 GHz.

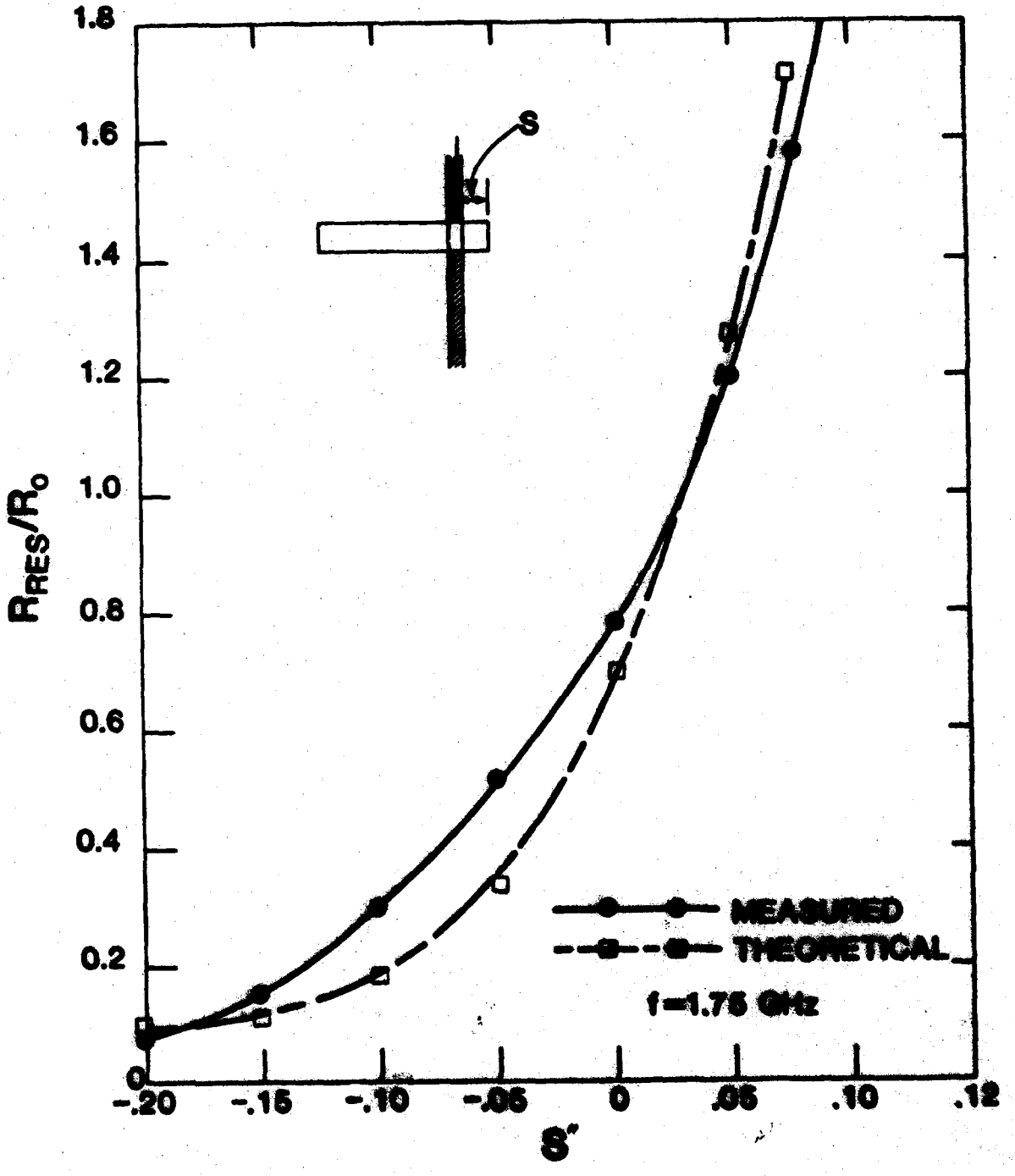

FIGURE 2.6 Normalized resonant slot resistance vs. offset.

APPENDIX A

UNIVERSITY OF CALIFORNIA

Los Angeles

MUTUAL COUPLING OF TWO SLOT ANTENNAS SEPARATED BY A SEPTUM

by

Panayotis John Gantayoumis

1961

TABLE OF CONTENTS

TABLE OF CONTENTS
(cont'd)

1. Introduction

One of the oldest techniques used to reduce mutual coupling between waveguide fed slots (as elements of phased array antennas) is the employment of conducting fences between slots and perpendicular to the ground plane. S. Edelberg and A. Oliner [1] give an evaluation of the effect of mutual coupling on the pattern and input admittance of an array and suggest the use of fences to reduce this effect. R. Mailloux [2] presents both theoretical and experimental studies of the power coupling of two parallel plate waveguides which radiate through a common ground plane with a thin metallic fence placed halfway in between. G. Franceschetti [3] uses plane wave expansion and Geometrical Theory of Diffraction (GTD) to deduce both the real and imaginary parts of the mutual admittance between two loosely coupled, infinitely long slots on a ground plane separated by a thin fence.

In this work the limitation of a thin fence is removed and the radius of curvature of the fence is taken into account by modeling the fence by a half cylinder of elliptic cross-section. Since the elliptic coordinate system is separable the exact solution to the problem can be derived.

The computer program evaluating the various eigenfunctions needed in the representation of the fields in the above mentioned coordinate system has been specially designed for scattering problems. Great care has been devoted to make the subroutines fast, accurate, simple to use and versatile. Also the program has been designed so that the extension to finite size slots can be handled by extension of the program. Some of the extensions have already been undertaken.

2. Mutual admittance between antennas

Assume antenna #1 is radiating in the presence of antenna #2. An exact evaluation of the mutual coupling in the general case can be achieved only by solving the associated boundary value problem and after proper definition of the driving point voltages and currents on the antennas. This procedure is in most practical cases, even the simpler ones, too complicated and several approximate techniques have been developed. Most of them require invisibility of the antennas (i.e., the radiation of any antenna in the system is not affected by the presence of any of the others). This requirement is met if the receiving antenna is located in the far field of the radiating antenna is located in the far field of the radiating antenna or if the receiving antenna is of negligible cross-section, as is the case with infinitesimally narrow slots considered in this thesis.

In this case we can write

$$I_1 = I_1 Y_{11} + V_2 Y_{12} \tag{1a}$$

$$I_2 = V_1 Y_{21} + V_2 Y_{22} \tag{1b}$$

where I,V are proper measures of the magnetic and electric field respectively in the slot aperture plane. The mutual admittance is given by

$$Y_{21} = \left. \frac{I_2}{V_1} \right|_{V_2 = 0} \tag{2}$$

The condition is equivalent to a shorted slot (the equivalent by an electric conductor). Since slot #2 was infinitesimally narrow this change will not affect the field (invisibility condition).

3. Transformation of the Y_{12} Problem to Scattering by an Elliptic Cylinder

As mentioned in the introductory section, the fence is modeled in terms of a half cylinder of elliptic cross-section (Figure 1). The slots are assumed to be of infinitesimal width and are modeled in terms of filamentary line currents. Of course the effect of a wider slot with known or assumed magnetic current distribution can be taken into account, but the effect is believed to be negligible for realistic cases of mutual admittance computation.

The problem is attacked by applying image theory and then by considering the scattering by an infinite perfectly conducting cylinder of elliptic cross-section in the presence of an infinite magnetic line source.

3.1. Modeling of the Radiating Slot

Let V_1 be the voltage across the slot which is assumed of infinitesimal width. The electric field across the slot is (refer to Figure 2)

$$E_z(z) = V_1 \delta(z + z_1)\hat{z}$$

By using Love's formulation of the equivalence principle, we can replace the tangential electric field by a magnetic surface current density and close the aperture with a perfect electric conductor, thus short circuiting the electric current density associated with the tangential magnetic field in the slot. The current density according to the equivalence principle will be

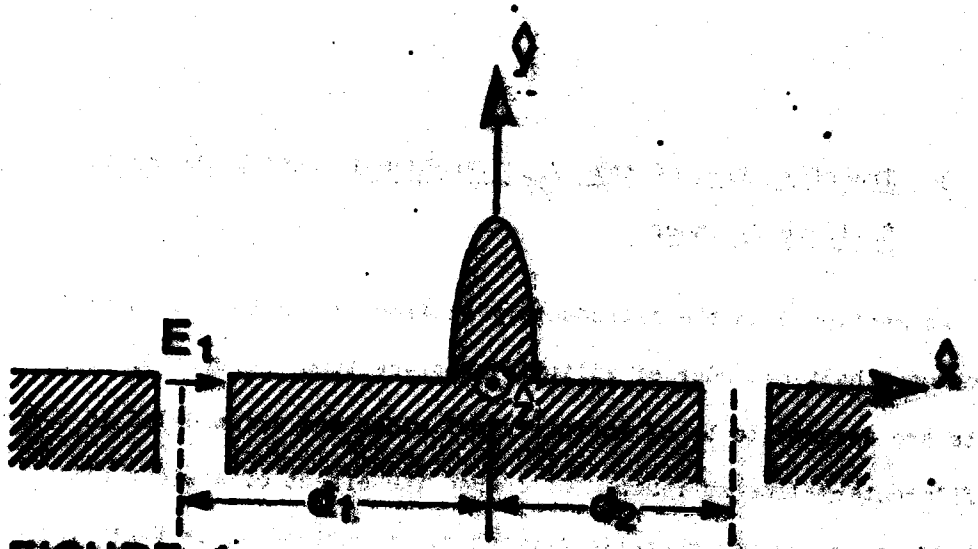

FIGURE 1
Model of the two slots separated by a metalic fence problem.

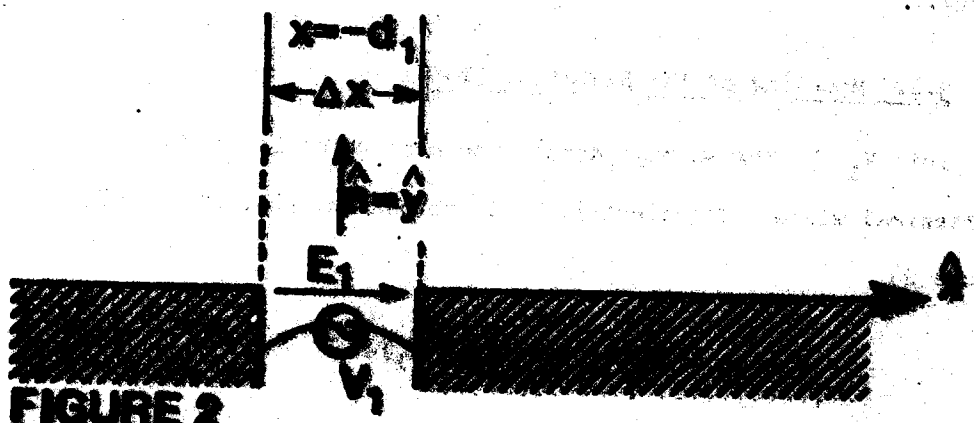

FIGURE 2
The radiating slot.

$$J_{ms} = -n \times E_1 = -\hat{Y} \times (V_1 \delta(x + d_1)\hat{x})$$
$$= \hat{z} V_1 \delta(x + d_1) = J_{zs} \delta(x + d_1) \tag{3}$$

as expected we get a magnetic line current of magnitude V_1 and directed along the positive z-axis (Figure 2).

3.2. Modeling the Receiving Slot

From the definition of mutual admittance between two slots (2) we get

$$Y_{21} = \frac{J_2}{v_1}\Big|_{v_2 = 0} \tag{4}$$

wherein J, v are proper measures of the magnetic and electric fields respectively in the slot aperture plane. For infinitesimaly narrow slots exited by TEM waves, J and v are the magnetic field along the slot and the voltage across the slot respectively. The condition $v_2 = 0$ is of course equivalent to a shorted slot. Thus (4) becomes

$$Y_{21} = \frac{H_{z2}}{V_1} \tag{5}$$

wherein H_{z2}, V_1 as depicted in Figure 4.

Using both the model for the transmitting and receiving slot we get

$$Y_{21} = \frac{H_{z2}}{V_1} \tag{6}$$

where H_{z2}, V_1 are as shown in Figure 5.

Now we are ready to apply image theory. The magnitude of the

source must be doubled, since the source and its image coincide, or alternatively the scattered field must be doubled since linearity holds. Thus the final expression for the mutual admittance is

$$Y_{21} = \frac{2I_{z2}}{V_1} \tag{7}$$

as shown in Figure 6.

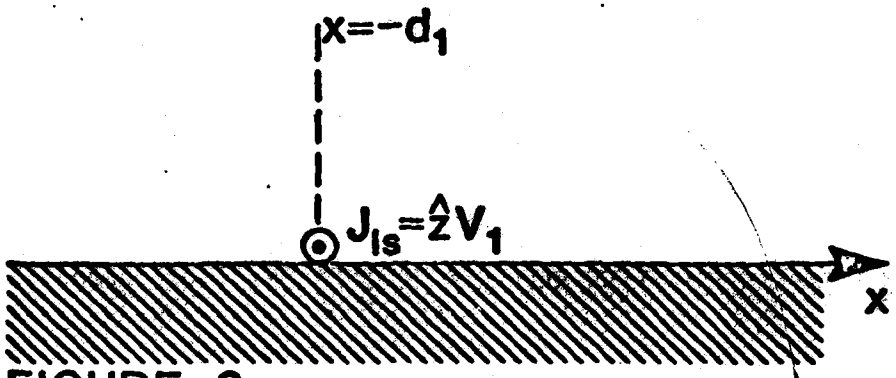

FIGURE 3
Model of the radiating slot.

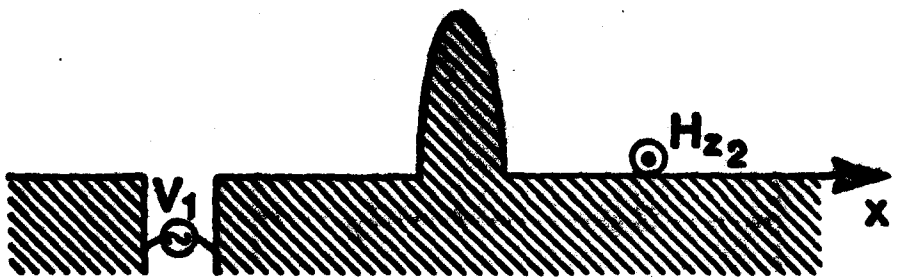

FIGURE 4

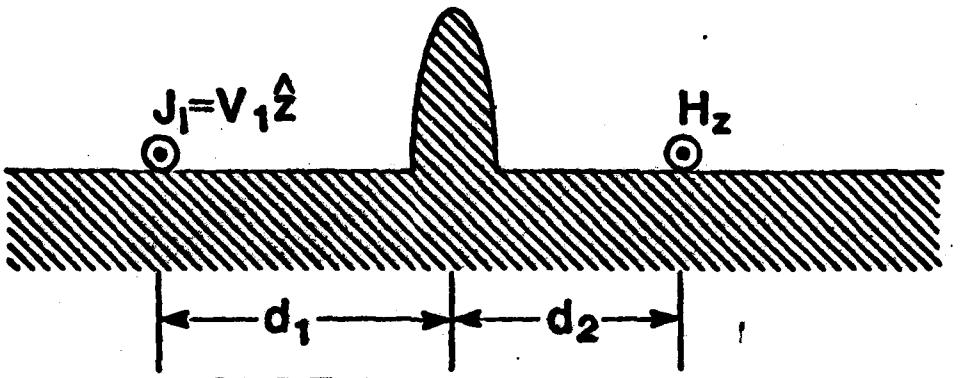

FIGURE 5

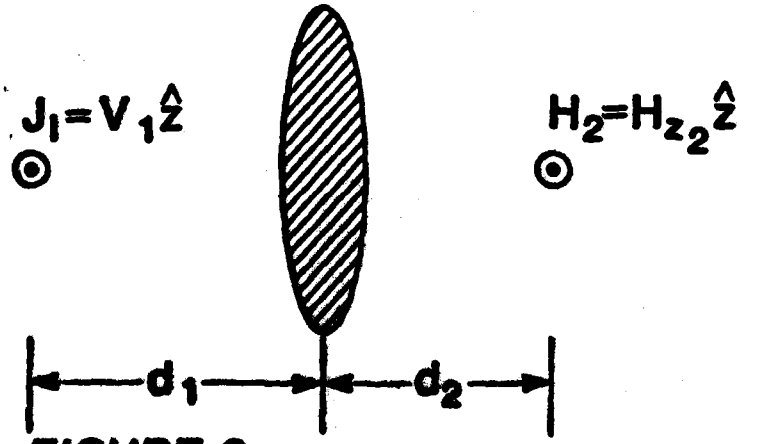

FIGURE 6
Final model.

4. Waves in Cylindrical Geometries

In a homogeneous isotropic medium without sources the electromagnetic fields can be derived from the Hertz vector potentials [4].

$$\mathbf{E} = \nabla\times\nabla\times\boldsymbol{\Pi} + j\omega\mu\nabla\times\boldsymbol{\Pi}_m \tag{8a}$$

$$\mathbf{H} = -j\omega\mu\nabla\times\boldsymbol{\Pi} + \nabla\times\nabla\times\boldsymbol{\Pi}_m \tag{8b}$$

where $\boldsymbol{\Pi}, \boldsymbol{\Pi}_m$ are the Hertz vector potentials which satisfy the vector wave equation

$$\nabla\times\nabla\times\boldsymbol{\Pi} - \nabla\nabla\cdot\boldsymbol{\Pi} + k^2\boldsymbol{\Pi} = 0. \tag{9}$$

In a cylindrical system generated by the translation of a line parallel to the z-axis, the z-components of the Hertz potentials are enough to generate the fields. The $\Pi_z\hat{z}$ vector gives rise to TM solutions (those with $H_z = 0$) while the $\Pi_{mz}\hat{z}$ vector to TE solutions ($E_z = 0$). Use the notation of Stratton [4] to derive the components of E and H from (8) (assume $\partial/\partial z = 0$).

TM solutions.

$$E_1 = E_2 = 0 \tag{10a, 10b}$$

$$E_z = -\frac{1}{h_1 h_2}\left[\frac{\partial}{\partial u_1}\left(\frac{h_2}{h_1}\frac{\partial \Pi_z}{\partial u_1}\right) + \frac{\partial}{\partial u_2}\left(\frac{h_1}{h_2}\frac{\partial \Pi_z}{\partial u_2}\right)\right] = k^2\Pi_z \tag{10c}$$

$$H_1 = -\frac{j\omega\varepsilon}{h_2}\frac{\partial \Pi_z}{\partial u_2}\,;\quad H_2 = \frac{j\omega\varepsilon}{h_1}\frac{\partial \Pi_z}{\partial u_1} \tag{11a, 11b}$$

$$H_z = 0. \tag{11c}$$

Π_z satisfies following wave equation

$$\nabla^2 \Pi_z + k^2 \Pi_z = 0 \qquad (12)$$

$$\frac{1}{h_1 h_2} \frac{\partial}{\partial u_1} \left(\frac{h_2}{h_1} \frac{\partial \Pi_z}{\partial u_1} \right) + \frac{1}{h_1 h_2} \frac{\partial}{\partial u_2} \left(\frac{h_1}{h_2} \frac{\partial \Pi_z}{\partial u_2} \right) + k^2 \Pi_z = 0$$

<u>TE solutions</u>.

$$H_1 = H_2 = 0 \qquad (13a,13b)$$

$$H_z = -\frac{1}{h_1 h_2} \left[\frac{\partial}{\partial u_1} \left(\frac{h_2}{h_1} \frac{\partial \Pi_{mz}}{\partial u_1} \right) + \frac{\partial}{\partial u_2} \left(\frac{h_1}{h_2} \frac{\partial \Pi_{mz}}{\partial u_2} \right) \right] = k^2 \Pi_{mz} \qquad (13c)$$

$$E_1 = \frac{j\omega\mu}{h_2} \frac{\partial \Pi_{mz}}{\partial u_2} \qquad E_2 = -\frac{j\omega\mu}{h_1} \frac{\partial \Pi_{mz}}{\partial u_1} \qquad (14a,14b)$$

$$E_z = 0 \qquad (14c)$$

and Π_{mz} satisfies the same wave equation as Π_z. In our case neither the source nor the scatterer produce a z-directed component of the Electric field, thus we can expand our fields solely in terms of TE waves.

<u>4.1. The Incident Field</u>.

In the absence of the scatterer, and because of the axial symmetry, the best way to represent the fields is in circular cylindrical waves, centered at the source. For this case the parameters $u_1 = r$, $u_2 = \theta$, h_1 and h_2 are [4]

$$u_1 = r,\ u_2 = \theta;\ h_1 = 1;\ h_2 = r. \qquad (15a-d)$$

The wave equation (12) reduces to

$$\frac{1}{r}\frac{\partial}{\partial r}\left(r\frac{\partial}{\partial r}\Pi_{mz}\right)+\frac{1}{r^2}\frac{\partial^2}{\partial\theta^2}\Pi_{mz}+k^2\Pi_{mz}=0. \tag{16}$$

Due to the axial symmetry $\partial/\partial\theta = 0$ so that the solution is in terms of the well known Bessel functions of zeroth order.

The time dependence is $e^{-j\omega t}$ so that the appropriate representation of an outgoing wave is in terms of the Hankel function of the first kind

$$\Pi_{mz} = CH_0^{(1)}(kr). \tag{17}$$

The excited fields can be written as

$$E_1 = E_r = \frac{j\omega\mu}{r}\frac{\partial}{\partial\theta}\Pi_{mz} = 0 \tag{18a}$$

$$E_2 = E_\theta = -\frac{j\omega\mu}{1}\frac{\partial}{\partial r}\Pi_{mz} = -j\omega\mu C\frac{d}{dr}\left[H_0^{(1)}(kr)\right] \tag{18b}$$

$$H_z = k^2\Pi_{mz} = k^2CH_0^{(1)}(kr) \tag{19a}$$

$$H_r = H_\theta = 0 \tag{19b,19c}$$

To determine the constant C we shall use the relation

$$\lim_{r\to 0}\oint E_\theta r d\theta = -J_g = -V_1 \tag{20}$$

since

$$E_\theta = -j\omega\mu C\frac{d}{dr}\left[H_0^{(1)}(kr)\right] \tag{21a}$$

and

$$H_0^{(1)}(kr) \xrightarrow[r\to 0]{} \frac{2j}{\pi r} \tag{21b}$$

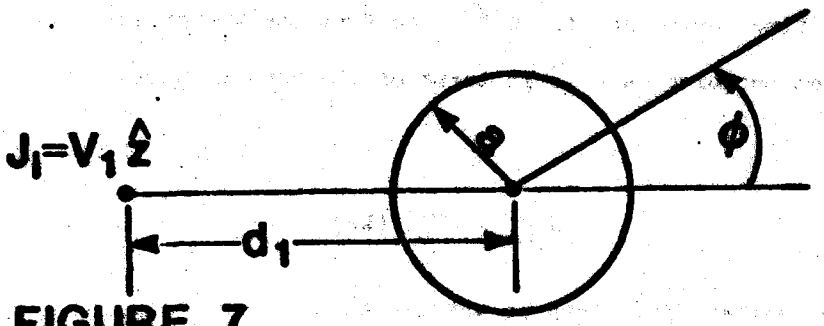

FIGURE 7
Scattering by a circular cylinder.

thus

$$\lim_{r \to 0} H_0 = \frac{2\pi i C}{\nu r} \tag{21c}$$

The condition (20) reduces to

$$\oint \frac{2\pi i C}{\nu} d\theta = -V_1 \tag{22}$$

or

$$C = -\frac{V_1}{4\pi i}. \tag{23}$$

Substitute the value of C into (22a)

$$H_0 = -\frac{V_1 k^2}{4\pi i} H_0^{(1)}(kr). \tag{24}$$

4.2. The Green's Function in Circular Cylindrical Coordinate System.

As an easy introduction to the elliptic cylindrical Green's function the circular case is considered. It is also a limiting case of an elliptic cylinder becoming a circular cylinder.

The situation depicted in Figure 7 consists of a circular cylinder of radius a and an infinitely long magnetic current source at distance d_1. The incident field is

$$H_0^i = -\frac{V_1 k^2}{4\pi i} H_0^{(1)}(k|r - d_1|). \tag{25}$$

For $r < d_1$ we have, by the addition theorem for Hankel functions,

$$H_0^i = -\frac{V_1 k^2}{4\pi i} \sum_{n=-\infty}^{\infty} H_n^{(1)}(kd_1) J_n(kr) e^{in(\theta - \tau)}. \tag{26}$$

The scattered field will be a superposition of outgoing waves of the type

$$H_n^{(1)}(kr)e^{jn\phi}. \tag{27}$$

Thus the scattered field takes the form

$$E_z^s = -\frac{V_2 k^2}{4\omega\epsilon} \sum_{n=-\infty}^{\infty} C_n H_n^{(1)}(kd_1) H_n^{(1)}(kr) e^{jn\phi} e^{-j\omega t}. \tag{28}$$

Since the coefficients C_n are not defined this expansion is not restrictive.

The associated incident and scattered electric fields are

$$E_\phi^i = \frac{jV_2}{4} \sum_{n=-\infty}^{\infty} H_n^{(1)}(kd_1) \frac{d}{dr}[J_n(kr)] e^{jn(\phi-\tau)} \tag{29}$$

and

$$E_\phi^s = \frac{jV_2}{4} \sum C_n H_n^{(1)}(kd_1) \frac{\partial}{\partial r}[H_n^{(1)}(kr)] e^{jn(\phi-\tau)}. \tag{30}$$

From the preceding two equations it is evident that

$$C_n = -\left.\frac{\frac{\partial}{\partial r}[J_n(kr)]}{\frac{\partial}{\partial r}[H_n^{(1)}(kr)]}\right|_{r=d} = -\frac{J_n'(kd)}{H_n^{(1)'}(kd)} \tag{31}$$

satisfies the boundary condition $E_\phi = E_\phi^i + E_\phi^s = 0$ on the cylinder surface. Thus the final solution is

$$E_z^s = \frac{V_2 k^2}{4\omega\epsilon} \sum_{n=-\infty}^{\infty} \frac{J_n'(kd)}{H_n^{(1)'}(kd)} H_n^{(1)}(kd_1) H_n^{(1)}(kr) e^{jn\phi} e^{-j\omega t} \tag{32}$$

and

$$H_z = H_z^i + H_z^s =$$

$$= -\frac{V_1 k^2}{4\omega\mu} H_0^{(1)}(k|r - d_1|) -$$

$$\sum_{n=-\infty}^{\infty} \frac{J_n'(ka)}{H_n^{(1)'}(ka)} H_n^{(1)}(kd_2) H_n^{(1)}(kr) e^{jn\phi} e^{-jn\gamma}. \qquad (33)$$

An alternative way to write the series is obtained with the use of the relations

$$J_{-n}(x) = (-1)^n J_n(x) \qquad (34a)$$

$$H_{-n}^{(1)}(x) = (-1)^n H_n^{(1)}(x). \qquad (34b)$$

The series now becomes

$$\sum_{n=-\infty}^{\infty} \frac{J_n'(ka)}{H_n^{(1)'}(ka)} H_n^{(1)}(kd_1) H_n^{(1)}(kr) e^{jn(\phi-\gamma)} =$$

$$= \frac{J_0'(ka)}{H_0^{(1)'}(ka)} H_0^{(1)}(kd_1) H_0^{(1)}(kr) +$$

$$2 \sum_{n=1}^{\infty} \frac{J_n'(ka)}{H_n^{(1)'}(ka)} H_n^{(1)}(kd_1) H_n^{(1)}(kr) \cos(n\gamma) \qquad (35)$$

The mutual coupling can now be evaluated

$$Y_{12} = -\frac{k}{2\zeta} \left[H_0^{(2)}[k(d_1 + d_2)] - \frac{J_0'(ka)}{H_0^{(1)'}(ka)} H_0^{(1)}(kd_1) H_0^{(1)}(kd_2) - \right.$$

$$\left. - 2 \sum_{n=1}^{\infty} \frac{J_n'(ka)}{H_n^{(1)'}(ka)} H_n^{(1)}(kd_1) H_n^{(1)}(kd_2) \right]. \qquad (36)$$

4.3. The Elliptic Cylindrical Coordinate System

The elliptic cylindrical coordinates $(q_1,q_2,q_3) = (\xi,\eta,z)$ shown in Figure 8 are related to the rectangular cartesian coordinates by the transformation

$$x = a\xi\eta \tag{57a}$$

$$y = a\left(\pm\sqrt{(\xi^2-1)(1-\eta^2)}\right) \tag{57b}$$

$$z = z. \tag{57c}$$

The geometric meaning of ξ,η is

$$\xi = \frac{r_1+r_2}{2a}\,;\quad \eta = \frac{r_1-r_2}{2a} \tag{58a,58b}$$

wherein r_1,r_2 are depicted in Figure 8.

The coefficients h_1,h_2,h_3 are

$$h_1 = a\sqrt{\frac{\xi^2-\eta^2}{\xi^2-1}}\,;\quad h_2 = a\sqrt{\frac{\xi^2-\eta^2}{1-\eta^2}}\,;\quad h_3 = 1 \tag{59a-c}$$

From (57b) it is obvious that the unit cube corresponds to values of these parameters in the following range:

$$|\xi| \geq 1 \qquad |\eta| \leq 1. \tag{60a,60b}$$

Usually ξ,η are replaced by

$$\xi = \cosh u \tag{61a}$$

$$\eta = \cos v. \tag{61b}$$

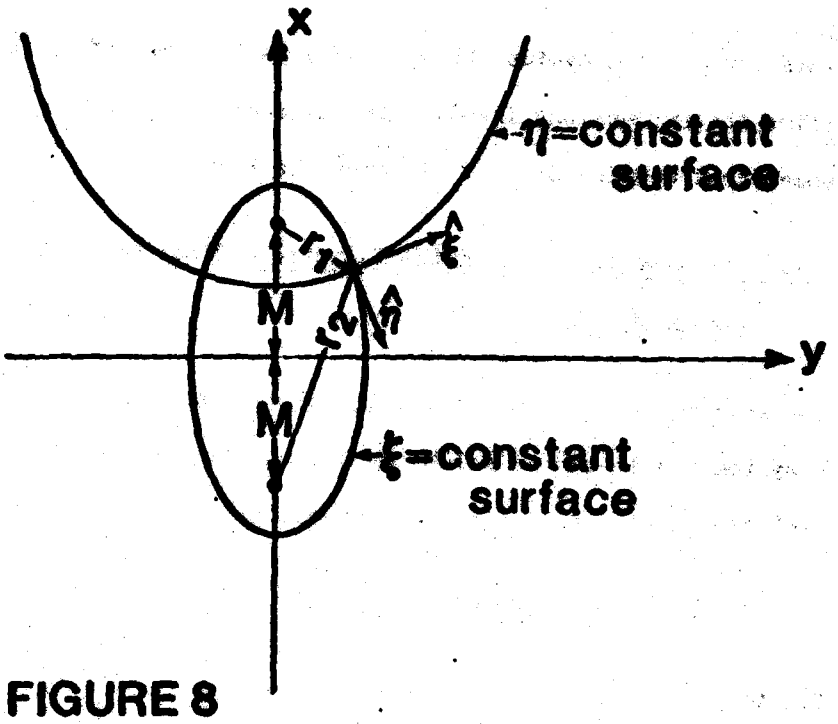

FIGURE 8

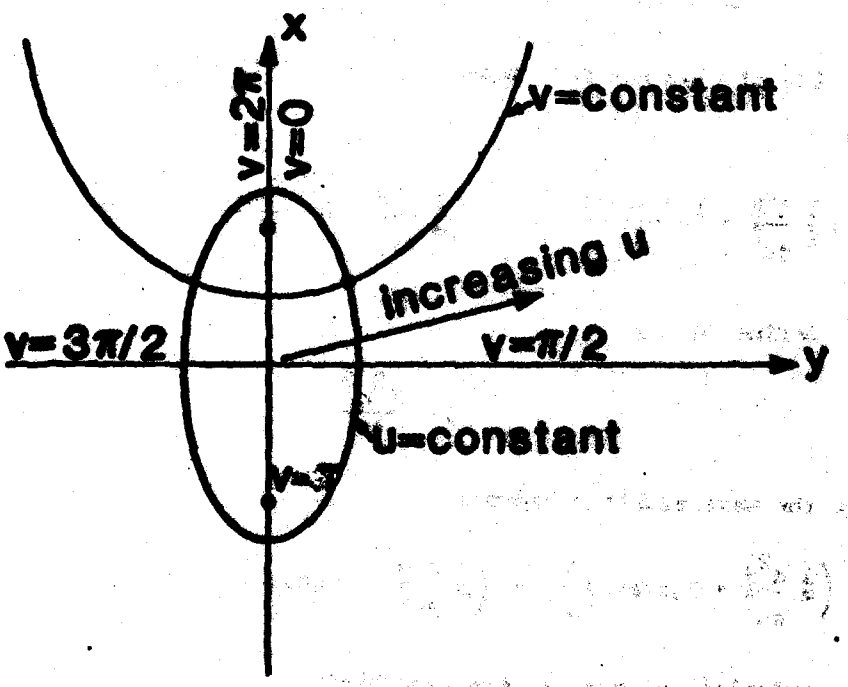

FIGURE 9

This replacement avoids the ambiguity in the sign of y and simplifies the expressions involved in the evaluation of the fields. The geometrical meaning of u,v is shown in Figure 9.

4.4. The Wave Equation in the Elliptic Cylindrical Coordinate System.

The wave equation is separable in the elliptic cylindrical coordinate system and it can be solved by the standard procedure. A basic solution of the following form is assumed

$$f(u,v) = R(u)\Theta(v). \tag{42}$$

The wave equation (12) can be written as

$$\frac{2}{k^2(\cosh 2u - \cos 2v)}\left(\frac{\partial^2}{\partial u^2} + \frac{\partial^2}{\partial v^2}\right) f + k^2 f = 0 . \tag{43}$$

Use of (39) has been made by substituting (42) into (43) one gets

$$\left(\frac{1}{R}\frac{d^2R}{du^2} + \frac{k^2h^2\cosh 2u}{2}\right) + \left(\frac{1}{\Theta}\frac{d^2\Theta}{dv^2} - \frac{k^2h^2\cos 2v}{2}\right) = 0 \tag{44}$$

Define q as

$$q = \frac{k^2h^2}{4} \tag{45}$$

then the wave equation becomes

$$\left(\frac{1}{R}\frac{d^2R}{du^2} + 2q\cosh 2u\right) + \left(\frac{1}{\Theta}\frac{d^2\Theta}{dv^2} - 2q\cos 2v\right) = 0 \tag{46}$$

The variables u and v are separated

$$\frac{1}{R}\frac{d^2R}{du^2} + 2q\cosh 2u = a \qquad (47a)$$

$$\frac{1}{\Theta}\frac{d^2\Theta}{dv^2} - 2q\cos 2v = -a \qquad (47b)$$

$$q = \frac{h^2k^2}{4} \qquad (47c)$$

a-being the separation constant.

The above equations can be written as

$$R'' - (a - 2q\cosh 2u)R = 0 \qquad (48a)$$

$$\Theta'' + (a - 2q\cos 2v)\Theta = 0. \qquad (48b)$$

The second equation is the well known Mathieu differential equation and the first one is usually referred to as the modified Mathieu equation.

The Mathieu differential equation needs closer attention since its solution must be a periodic function of v for the fields to be single valued (a rotation of 360 degrees around the cylinder brings us at the starting spot). The period can be either π or 2π. This requirement puts some restrictions on the values the separation constant a can take. It turns out that the separation constant can take values in four infinite sets, giving rise to four different types of solutions to both the Θ and R functions. These four types are labeled in this thesis as AE, AO, BE, BO.

The first letter stands for the kind of solution 'A' for even solutions and 'B' for odd solutions. The second letter stands for the periodicity of the solutions, 'E' for period of π and 'O' for

the period of 2π . Thus 'AE' is the class of all even solutions of period π.

The periodic solutions of the angular equation are

$$T_{xx_n}(v)$$

while the solutions of the radial equation are

$$J_{xx_n}(u),\ Y_{xx_n}(u),\ H^{(1)}_{xx_n}(u),\ H^{(2)}_{xx_n}(u)$$

where xx stands for one of AE, AO, BE, BO.

The representation of those functions in terms of other known functions can be found in [5].

4.5. Incident and Scattered Fields

The incident wave can be represented as [6]

$$H_z^i = -\frac{V_1 k^2}{4\omega\mu} H_0^{(1)}(k|\tau - d_1|) =$$

$$= -\frac{V_1 k^2}{\omega\mu} \sum_{xx = \substack{AE \\ AO \\ BE \\ BO}} \sum_{n=0}^{\infty} \frac{T_{xx_n}(u_0) T_{xx_n}(-\frac{\pi}{2})}{N_n^{xx}(q)} \cdot$$

$$\left\{ \begin{array}{l} J_{xx_n}(u_0) H^{(1)}(u);\ u > u_0 \\ J_{xx_n}(u) H^{(1)}(u_0);\ u_0 > u \end{array} \right\} \qquad (49)$$

Using the same method as for the circular cylindrical case we can find the scattered field to be

$$H_z^s = \frac{V_1 k^2}{\omega\mu} \sum_{xx} \sum_n \frac{T_{xx_n}(v) T_{xx_n}(-\frac{\pi}{2})}{M_n^{xx}(q)} \cdot$$

$$\frac{J'_{xx_n}(u_s)}{H^{(1)'}_{xx_n}(u_s)} H^{(1)}_{xx_n}(u_0) H^{(1)}_{xx_n}(u) \qquad (50)$$

where u_s corresponds to the scattering surface and u_0 to the source position (Figure 10).

Using the above relations we can finally express the mutual coupling as a function of the geometry

$$Y_{21} = \frac{2H_{z_2}}{V_1} = \frac{2(H^i_{z_2} + H^s_{z_2})}{V_1} =$$

$$= -\frac{k}{2z} H_0^{(1)}(k(d_1 + d_2)) -$$

$$4 \sum_{\substack{xx = AE \\ BO}} \sum_n \frac{T_{xx_n}(\frac{\pi}{2}) T_{xx_n}(-\frac{\pi}{2})}{M_n^{xx}(q)} \cdot$$

$$\cdot \frac{T'_{xx_n}(u_s)}{H^{(1)'}(u_s)} H^{(1)}_{xx_n}(u_0) H^{(1)}_{xx_n}(u)$$

Use of the following relation has been made

$$\frac{k^2}{2\omega\mu} = \frac{k\omega\sqrt{\mu\varepsilon}}{2\omega\mu} = \frac{k}{2z} .$$

And $M_n^{xx}(q)$ are normalizing factors, as defined in [5] or [6].

The dependence of the Mathieu functions on q is implied to simplify the notation.

5. Numerical Results

The coupling of two slots separated by metalic fence of elliptic cross-section is evaluated for several slot separations and fence dimensions (height, thickness). The exact solution is also compared against the limiting case when the fence becomes infinitesimaly thin. The GTD approximation was used in the latter case and the expressions were derived by Dr. G. Franceschetti.

5.1 Overview of the Numerical Results

The dependence of the magnitude of the mutual admittance on the slot separation for various values of the height and the thickness of the septum is depicted in Figures 10 through 12 and 13 through 16. Each figure in the first set (10-12) contains the curves corresponding to one height of the septum, so that the effect of the septum thickness can be determined. The figures in the second set contain the same curves but rearranged so that each figure contains curves corresponding to the same thickness of the septum so that the effect of the height can be displayed.

The dependence of the mutual conductance and mutual susceptance on the septum separation and the septum parameters is depicted in Figures 16 through 30. The same arrangement as for the mutual admittance holds.

In many cases the results are compared to the curves corresponding to the absence of the septum. Some figures also contain the limiting case when the thickness of the septum approaches zero. Those curves were obtained by the GTD method as described earlier.

Tables in pages 47 to 67 display the contribution of the various elliptic-cylindrical modes in the coupling. Also, the speed of convergence and the expected accuracy can be deduced from the same tables.

Conclusions

The magnitude and phase of the mutual admittance of two slots on the ground plane separated by a metallic fence has been evaluated and presented in this work. The exact solution in terms of the proper radial and angular functions has been found and programmed on the computer. An efficient and pseudointeractive program has also been created to fascilitate the use of an over 3000 statements long program. The cost to evaluate and plot the average curve in Figures 10 through 30 was estimated to $10 using an IBM 3033 computer operating under MVS.

The results could not be checked for accuracy against any other work because of the lack of any available reference but several tests have been made to insure the accuracy of the various functions and all summations have built-in numerical convergence tests which print various messages if an error is suspected. No such error occured during the computation of the published results. The tables included suggest an accuracy of about five digits. Because of the complexity of the algorithm a rigorous rounding and trancating error has not been performed.

As stated in the introductory section the results and the program itself will be used in the design of optimized phased slot arrays. The availability of more design parameters, namely the position, height and thickness of the septums is hoped to result in much better arrays, radiating both sum and difference patterns.

The reduction of the mutual coupling is a plus by itself, but the control over the position where the imaginary part of the mutual impedance vanishes is believed to be of great importance; and a key factor in the design of arrays.

Key To Figures 10 Through 30

Each figure in the set contains curves representing the same quantity (i.e. mutual conductance, mutual admittance or mutual susceptance) and are titled accordingly. All figures contain two or more curves. Each curve is labelled at the left side of the plot by a number. A note at the upper right hand side relates this number to the particular case.

If the curve corresponds to an elliptic cylindrical septum the AA and BB numbers are given. AA is the normalized height of the septum a/λ, while BB is its normalized half width b/λ.

If the curve corresponds to an infinitesimally thin septum, analyzed by the Geometrical Theory of Diffraction, only the AA number is given and the words 'GTD METHOD' are printed.

Finally, the curves corresponding to the absence of the septum are labelled by 'W/O SEPTUM'. Of course, no AA nor BB numbers are given.

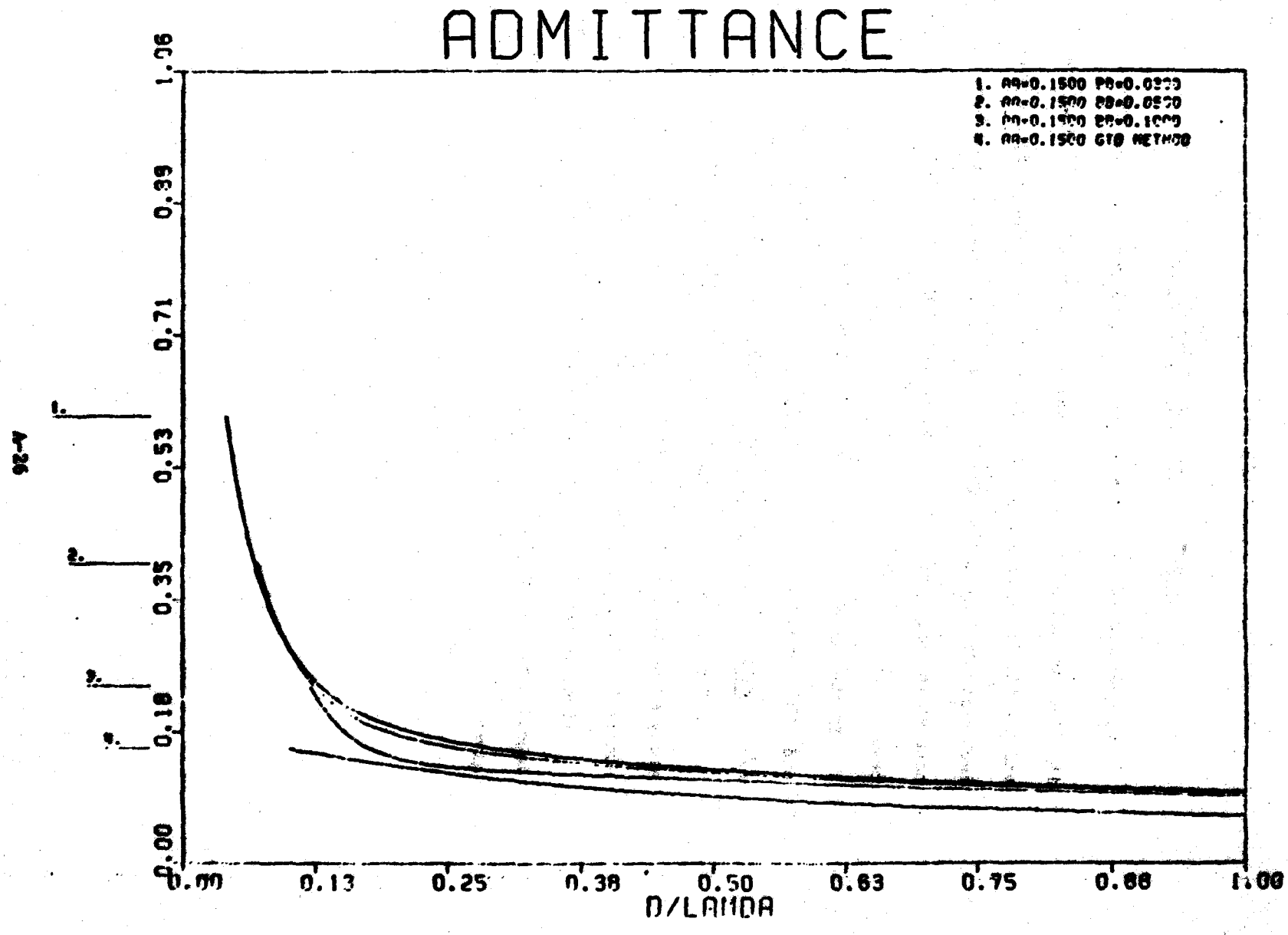
ADMITTANCE
1. AA=0.1500 BB=0.0000
2. AA=0.1500 BB=0.0500
3. AA=0.1500 BB=0.1000
4. AA=0.1500 GTD METHOD
1.06
0.89
0.71
0.53
0.35
0.18
0.00
0.00
0.13
0.25
0.38
0.50
0.63
0.75
0.88
1.00
D/LAMDA

Figure 10.

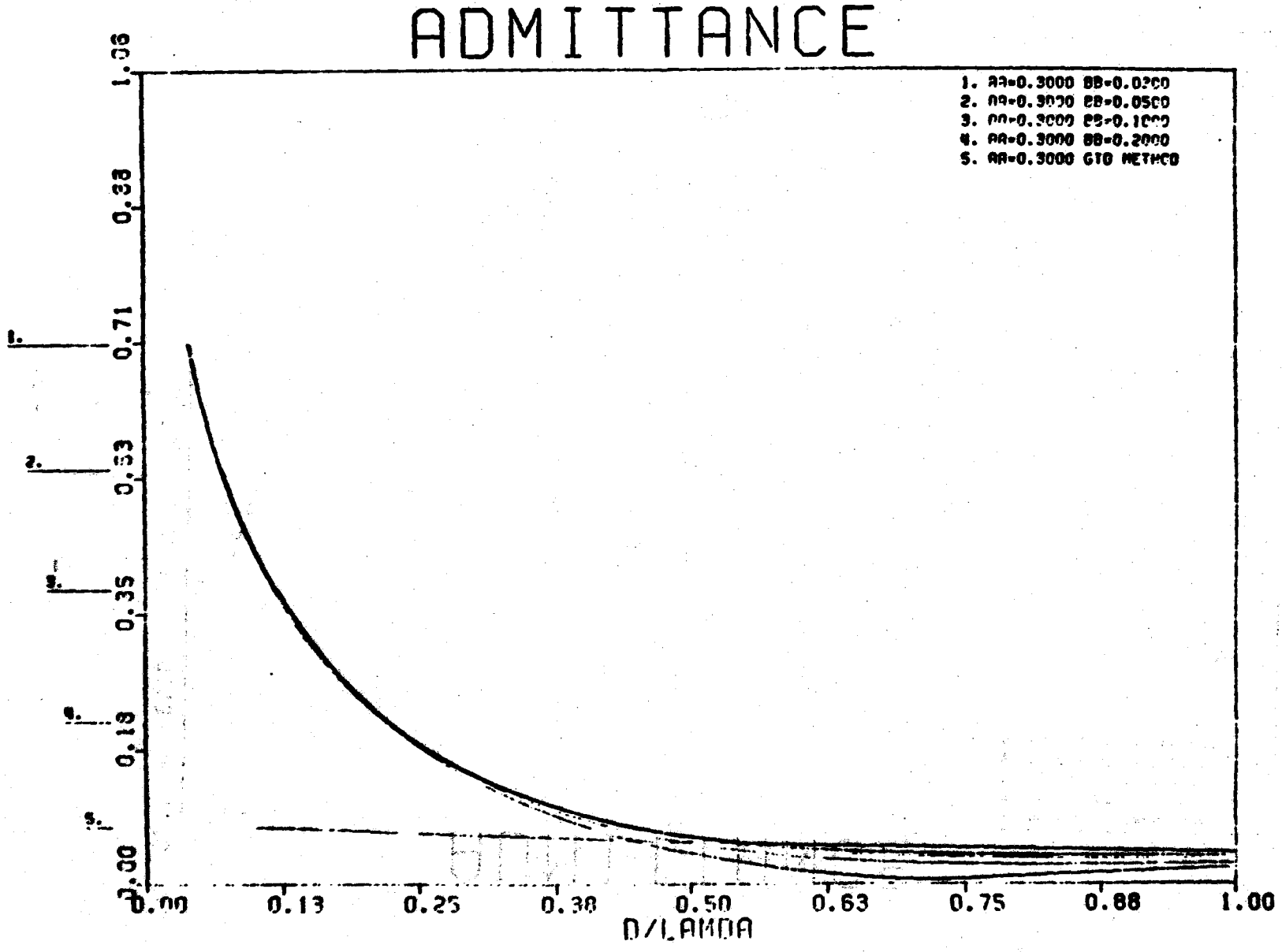
ADMITTANCE
1. AA=0.3000 BB=0.0500
2. AA=0.3000 BB=0.0500
3. AA=0.3000 BB=0.1000
4. AA=0.3000 BB=0.2000
5. AA=0.3000 GTD METHOD
1.06
0.88
0.71
0.53
0.35
0.18
0.00
0.00
0.13
0.25
0.38
0.50
0.63
0.75
0.88
1.00
D/LAMDA

Figure 11.

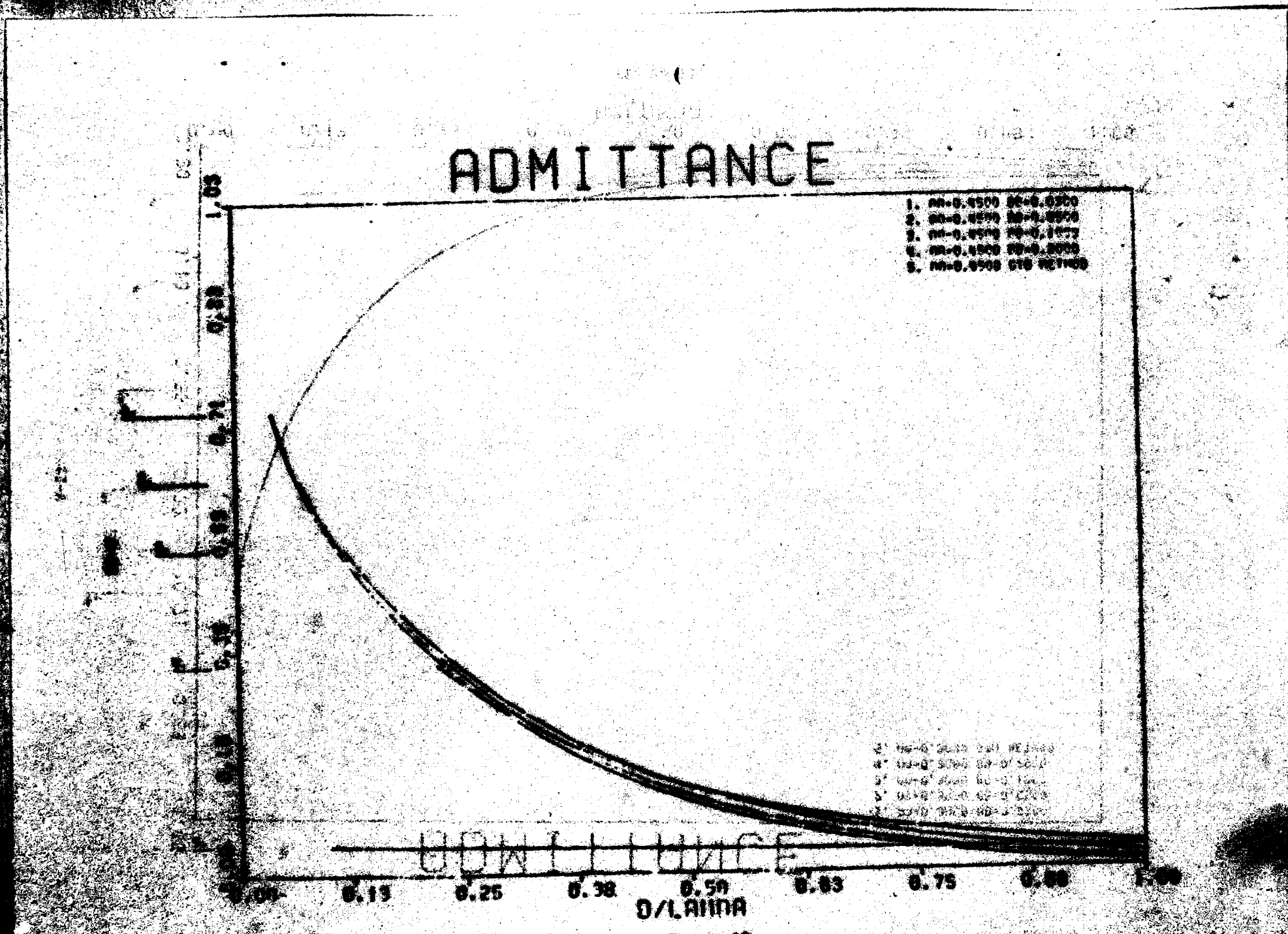

Figure 12.

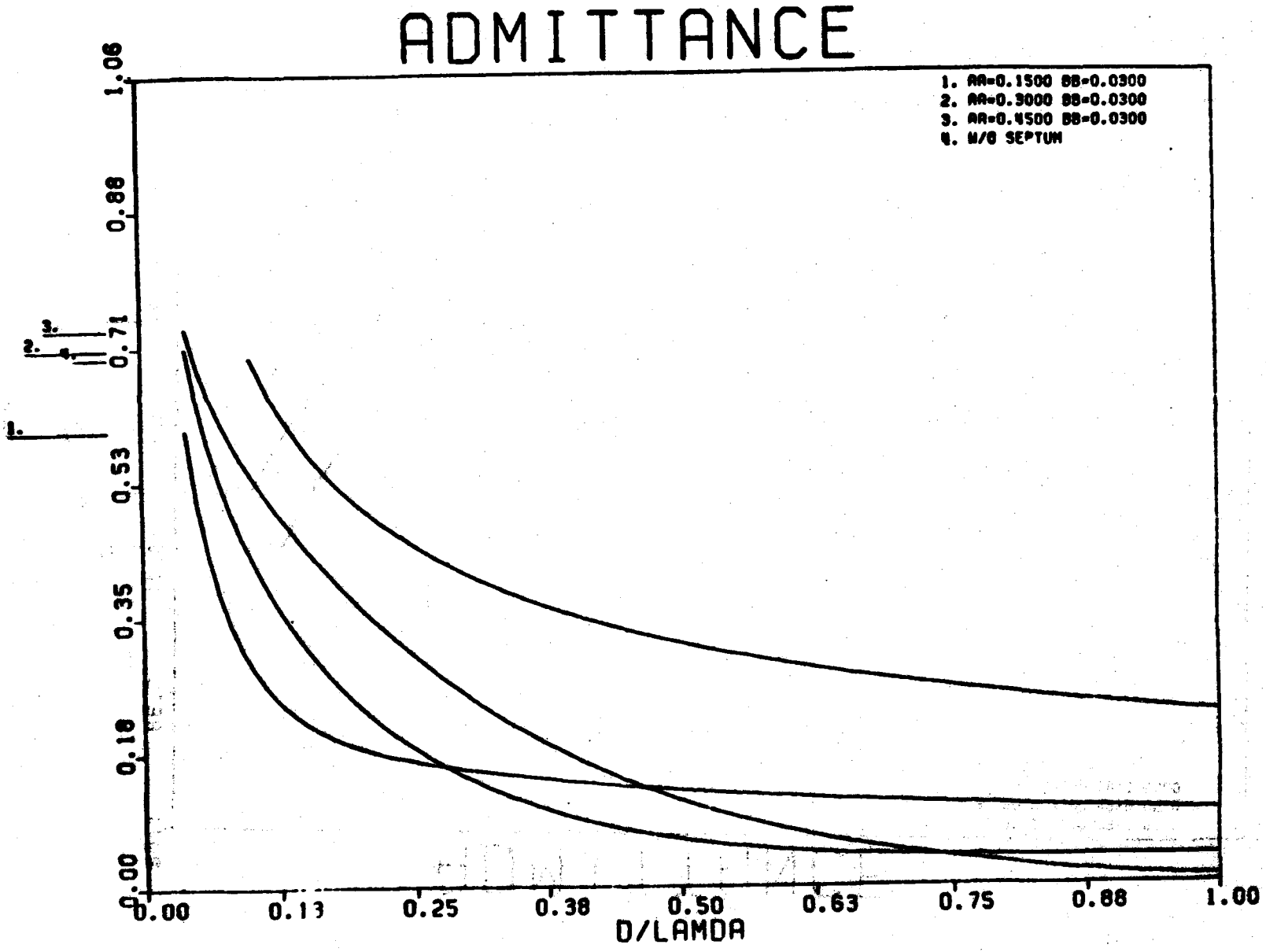
ADMITTANCE
1. AA=0.1500 BB=0.0300
2. AA=0.3000 BB=0.0300
3. AA=0.4500 BB=0.0300
4. W/O SEPTUM
1.06
0.88
0.71
0.53
0.35
0.18
0.00
0.00
0.13
0.25
0.38
0.50
0.63
0.75
0.88
1.00
D/LAMDA

Figure 13.

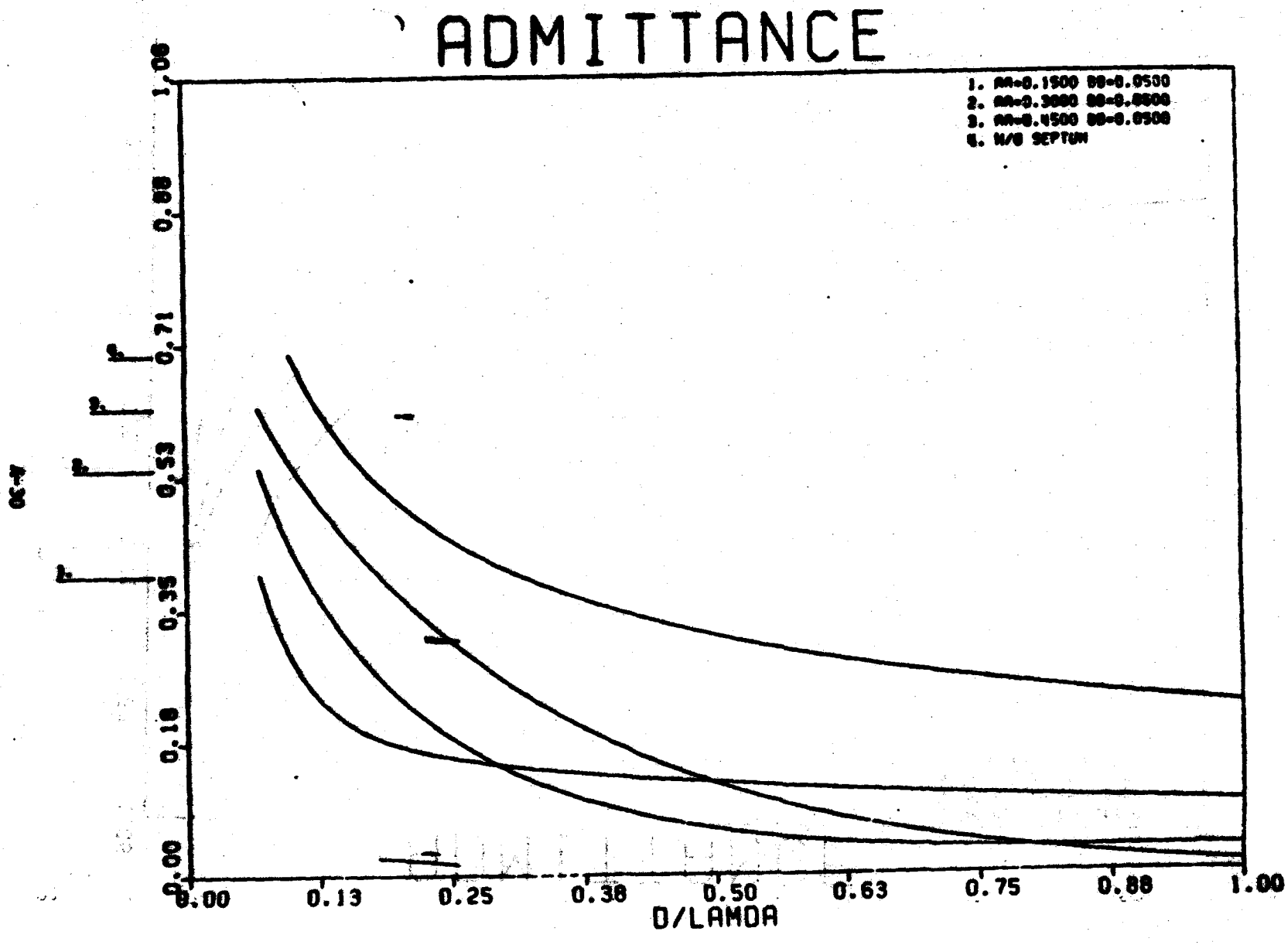
ADMITTANCE
1. AA=0.1500 BB=0.0500
2. AA=0.3000 BB=0.0000
3. AA=0.4500 BB=0.0500
4. W/O SEPTUM
1.00
0.88
0.71
0.53
0.35
0.18
0.00
0.00
0.13
0.25
0.38
0.50
0.63
0.75
0.88
1.00
D/LAMDA

Figure 14.

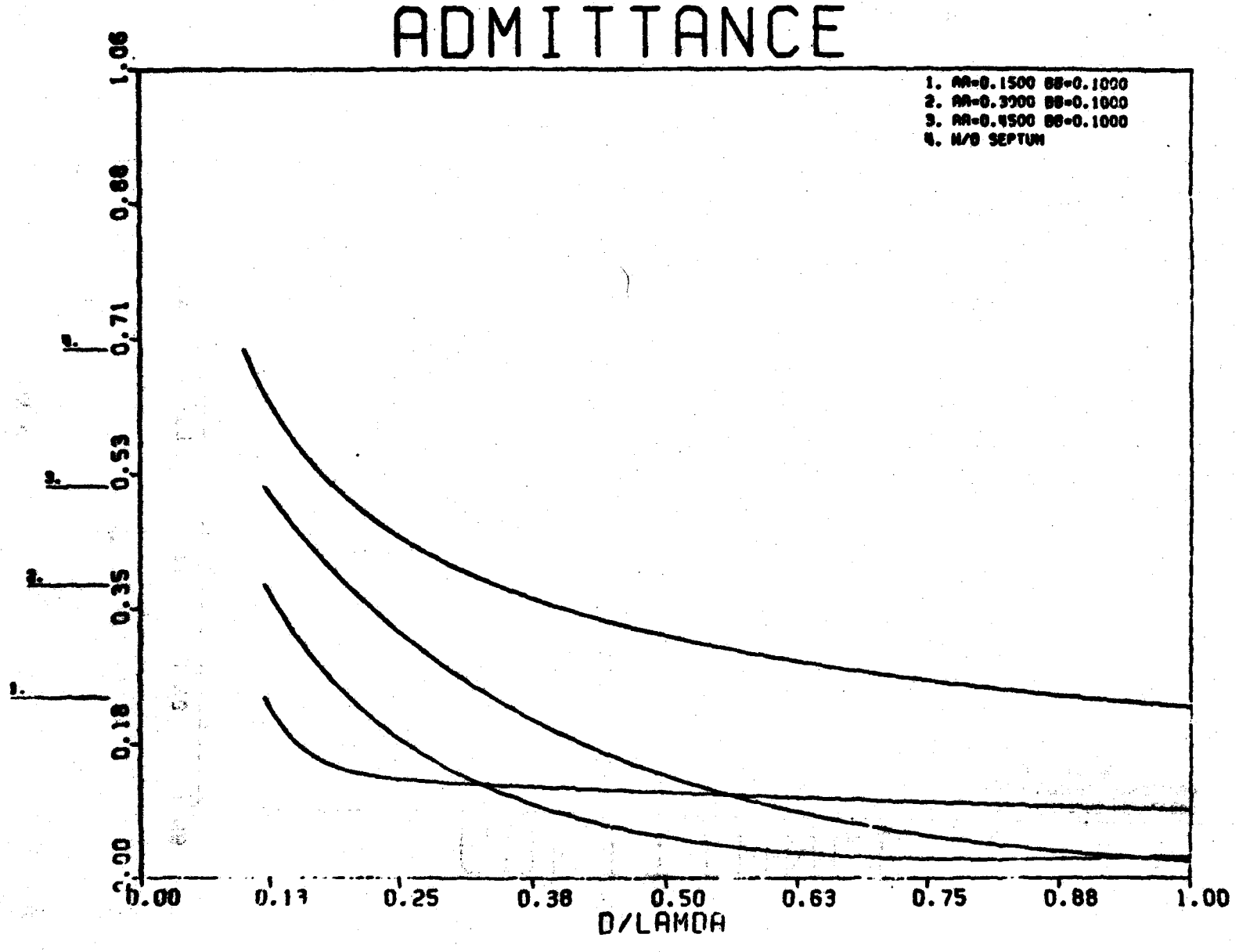
ADMITTANCE
1. AR=0.1500 BB=0.1000
2. AR=0.3000 BB=0.1000
3. AR=0.4500 BB=0.1000
4. H/O SEPTUM
1.06
0.88
0.71
0.53
0.35
0.18
0.00
0.00
0.13
0.25
0.38
0.50
0.63
0.75
0.88
1.00
D/LAMDA

Figure 15.

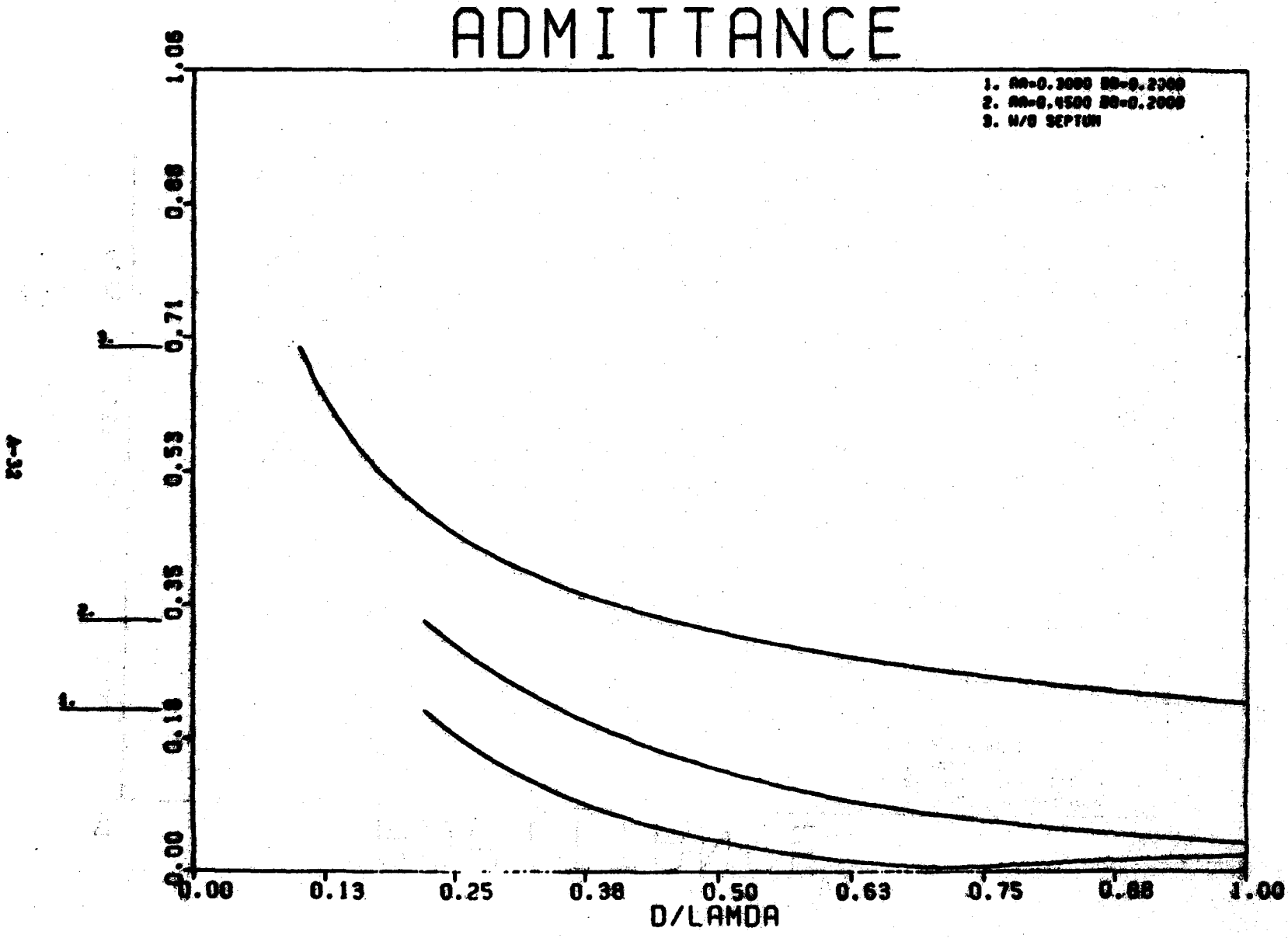
ADMITTANCE
1. AA=0.3000 BB=0.2300
2. AA=0.4500 BB=0.2000
3. H/B SEPTUM
1.06
0.88
0.71
0.53
0.35
0.18
0.00
0.00
0.13
0.25
0.38
0.50
0.63
0.75
0.88
1.00
D/LAMDA

Figure 16.

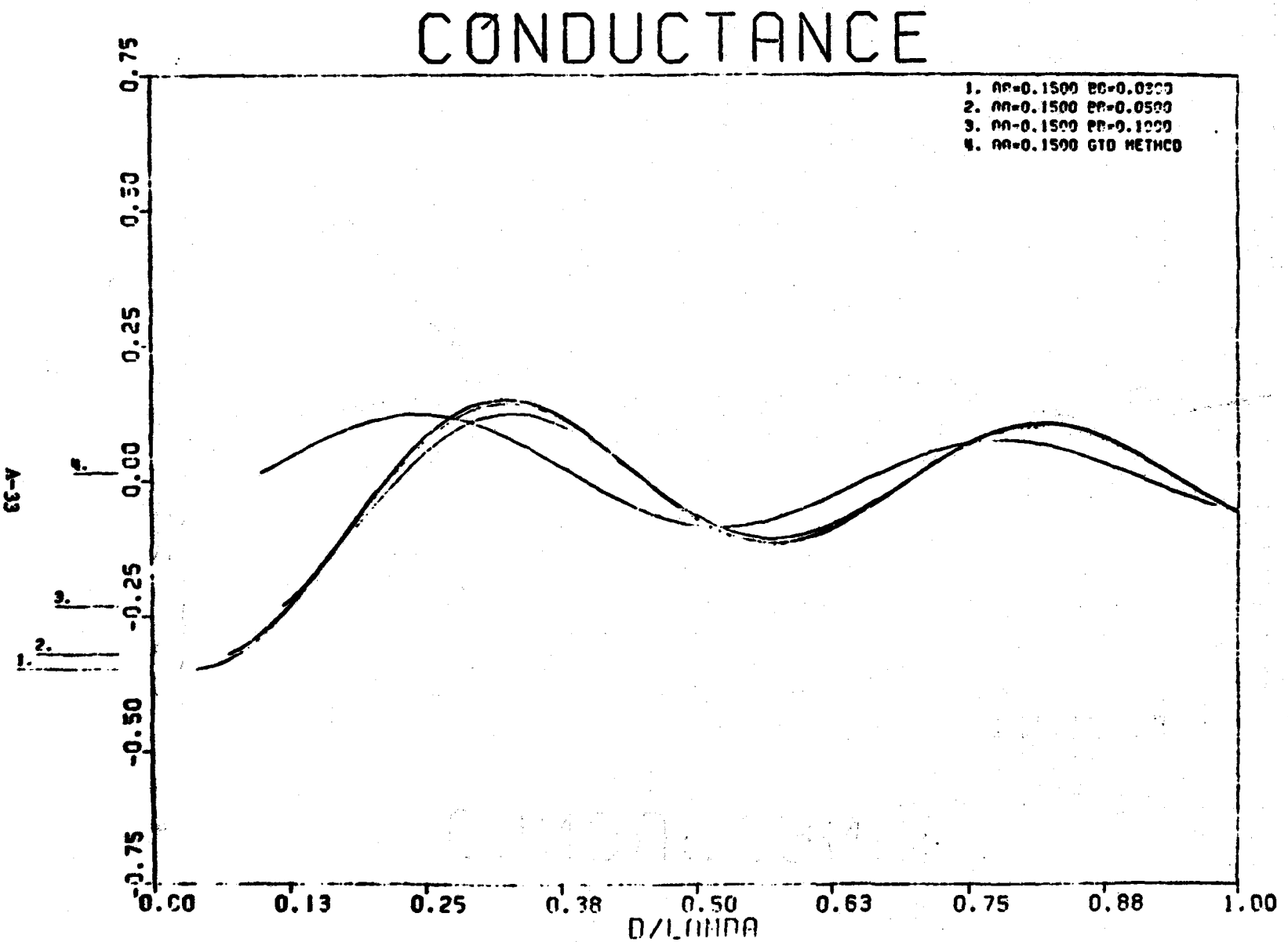
CONDUCTANCE
1. AA=0.1500 BB=0.0250
2. AA=0.1500 BB=0.0500
3. AA=0.1500 BB=0.1000
4. AA=0.1500 GTD METHOD
0.75
0.50
0.25
0.00
-0.25
-0.50
-0.75
0.00
0.13
0.25
0.38
0.50
0.63
0.75
0.88
1.00
D/LAMDA
A-33

Figure 17.

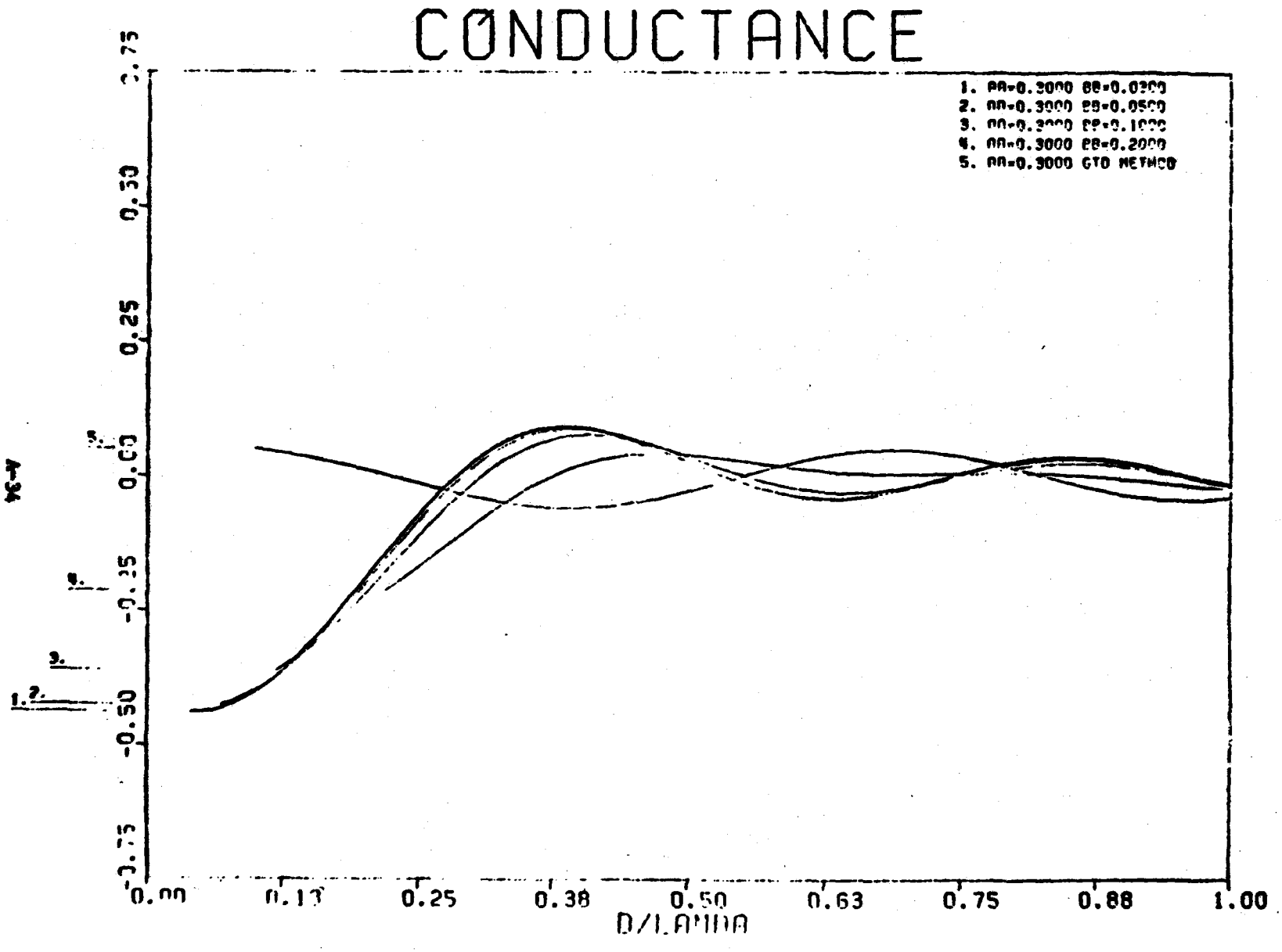
CONDUCTANCE
1. AA=0.3000 BB=0.0300
2. AA=0.3000 BB=0.0500
3. AA=0.3000 BB=0.1000
4. AA=0.3000 BB=0.2000
5. AA=0.3000 GTD METHOD
0.75
0.50
0.25
0.00
-0.25
-0.50
-0.75
0.00
0.13
0.25
0.38
0.50
0.63
0.75
0.88
1.00
D/LAMDA

Figure 18.

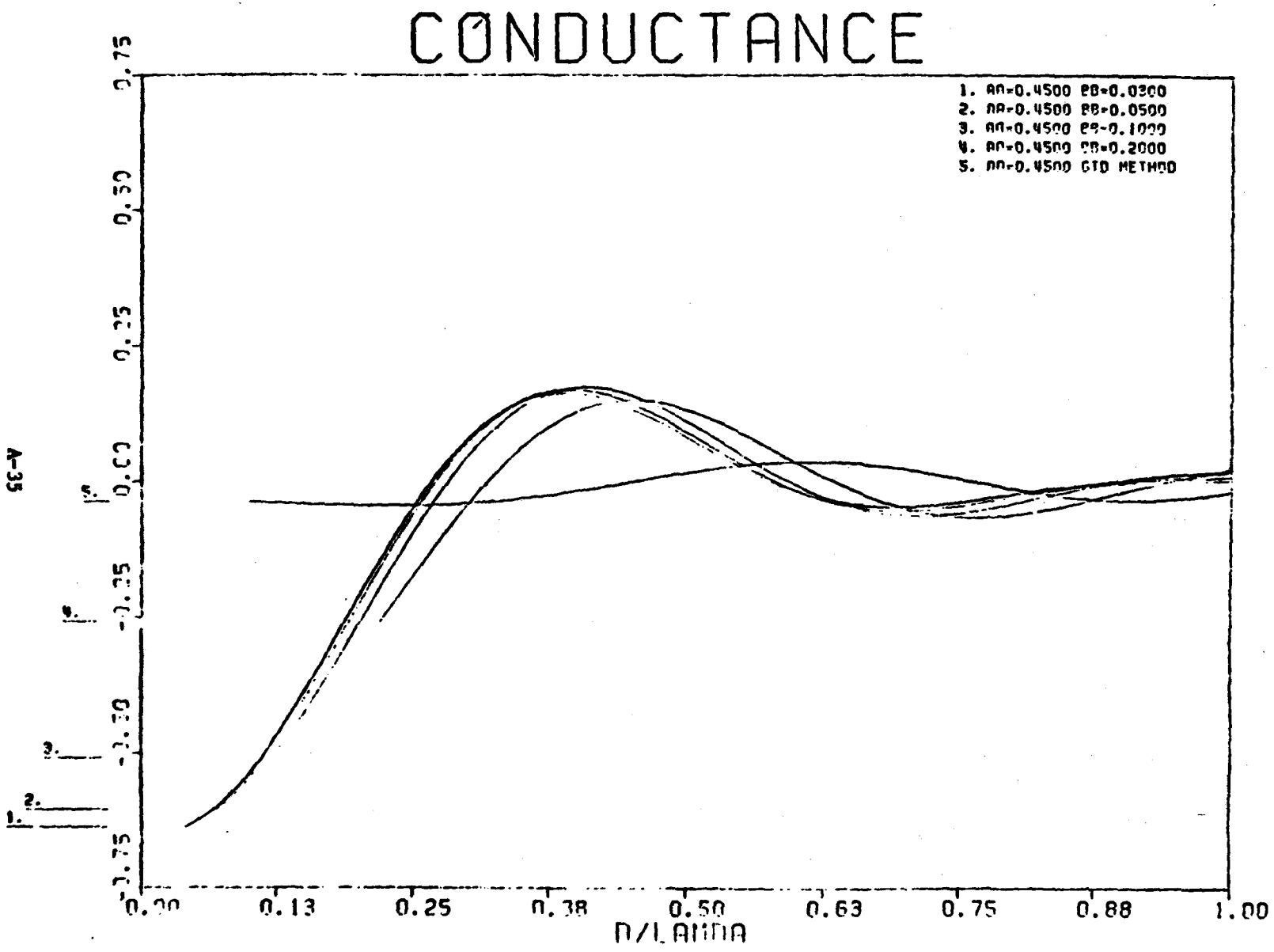
CONDUCTANCE
1. AA=0.4500 BB=0.0300
2. AA=0.4500 BB=0.0500
3. AA=0.4500 BB=0.1000
4. AA=0.4500 BB=0.2000
5. AA=0.4500 GTD METHOD
0.75
0.50
0.25
0.00
-0.25
-0.50
-0.75
0.00
0.13
0.25
0.38
0.50
0.63
0.75
0.88
1.00
D/LAMDA

Figure 19.

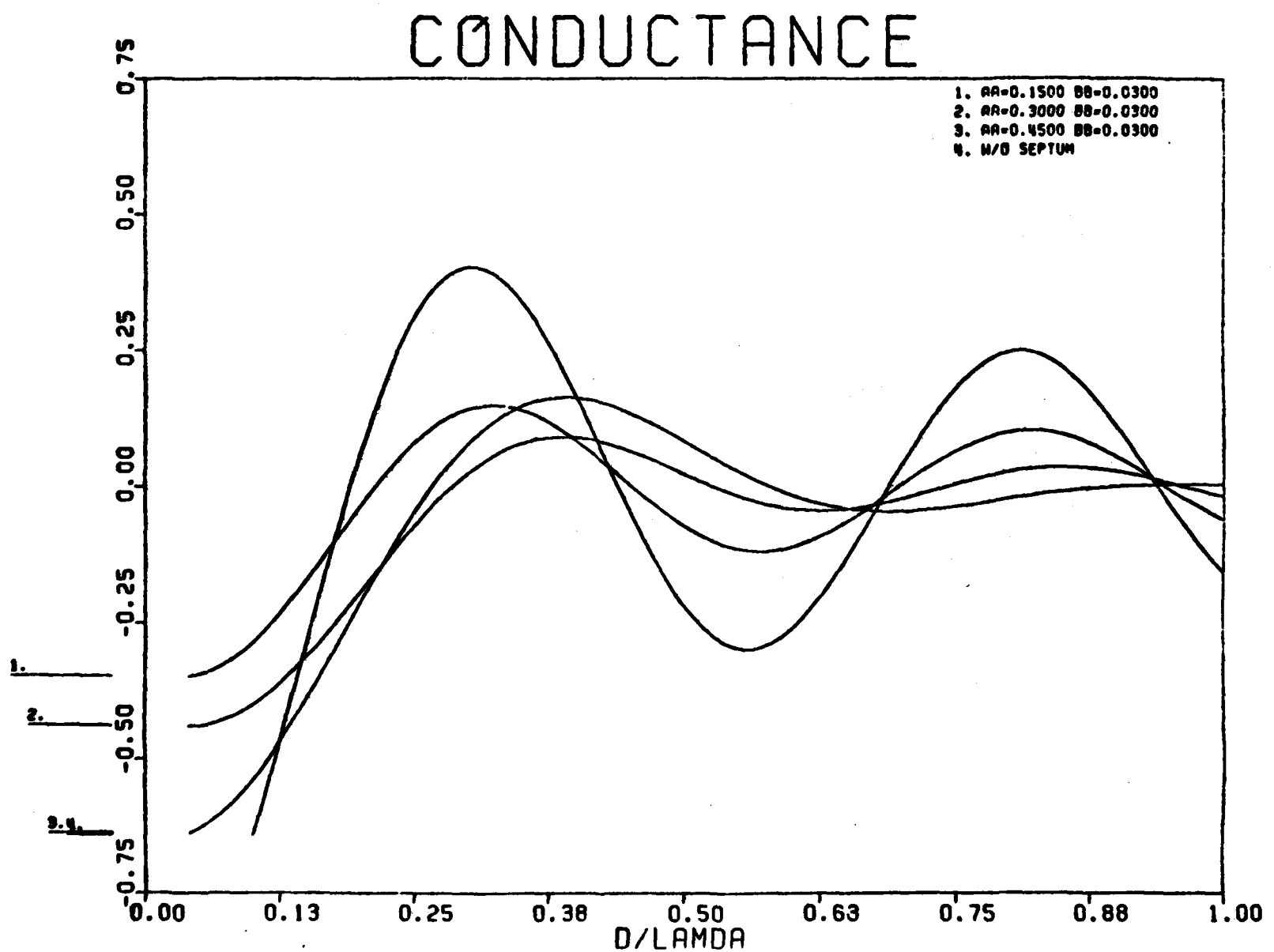
CONDUCTANCE
1. AA=0.1500 BB=0.0300
2. AA=0.3000 BB=0.0300
3. AA=0.4500 BB=0.0300
4. W/O SEPTUM
0.75
0.50
0.25
0.00
-0.25
-0.50
-0.75
0.00
0.13
0.25
0.38
0.50
0.63
0.75
0.88
1.00
D/LAMDA
1.
2.
3.4.

Figure 20.

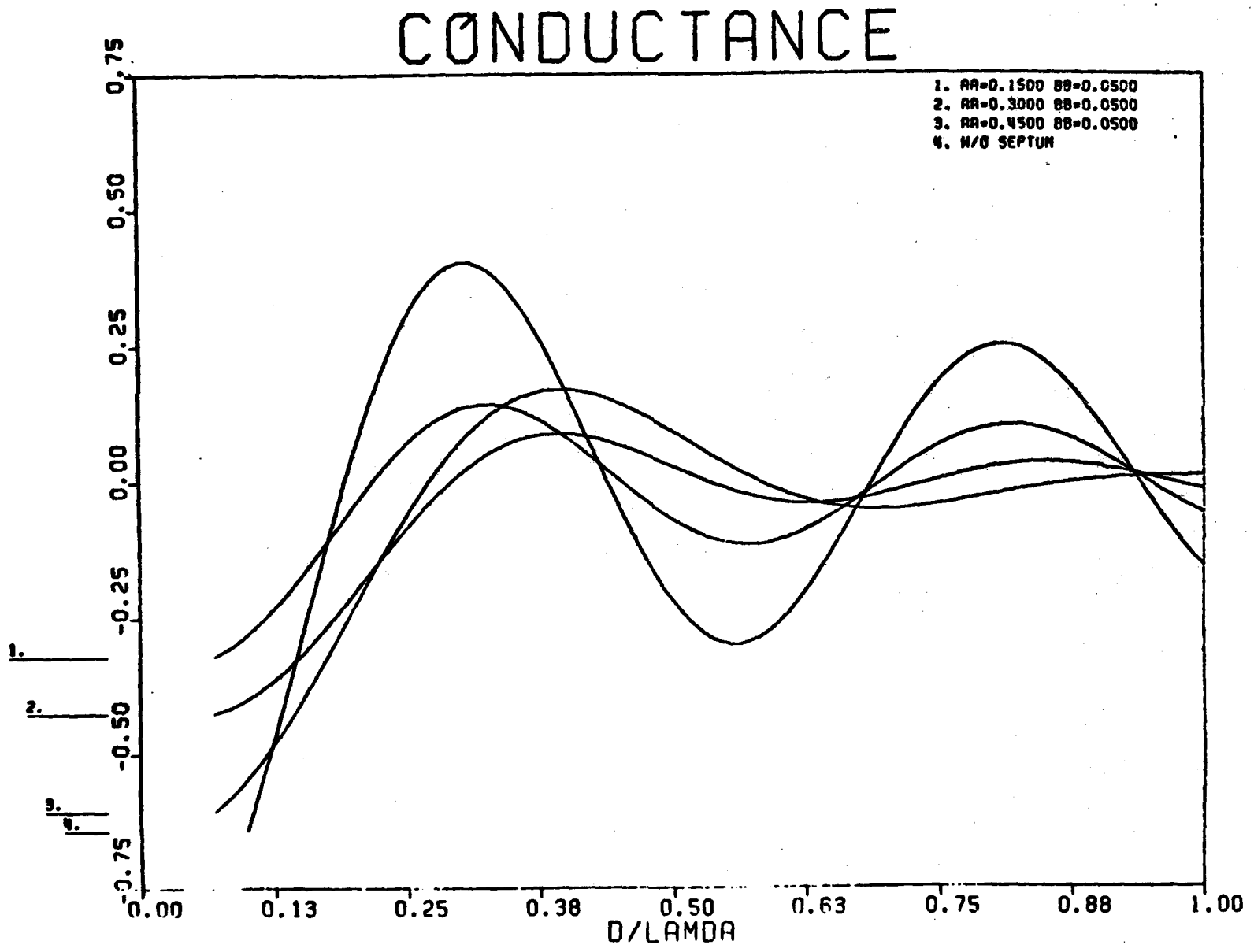
CONDUCTANCE
1. AA=0.1500 BB=0.0500
2. AA=0.3000 BB=0.0500
3. AA=0.4500 BB=0.0500
4. W/O SEPTUM
0.75
0.50
0.25
0.00
-0.25
-0.50
-0.75
0.00
0.13
0.25
0.38
0.50
0.63
0.75
0.88
1.00
D/LAMDA
1.
2.
3.
4.

Figure 21.

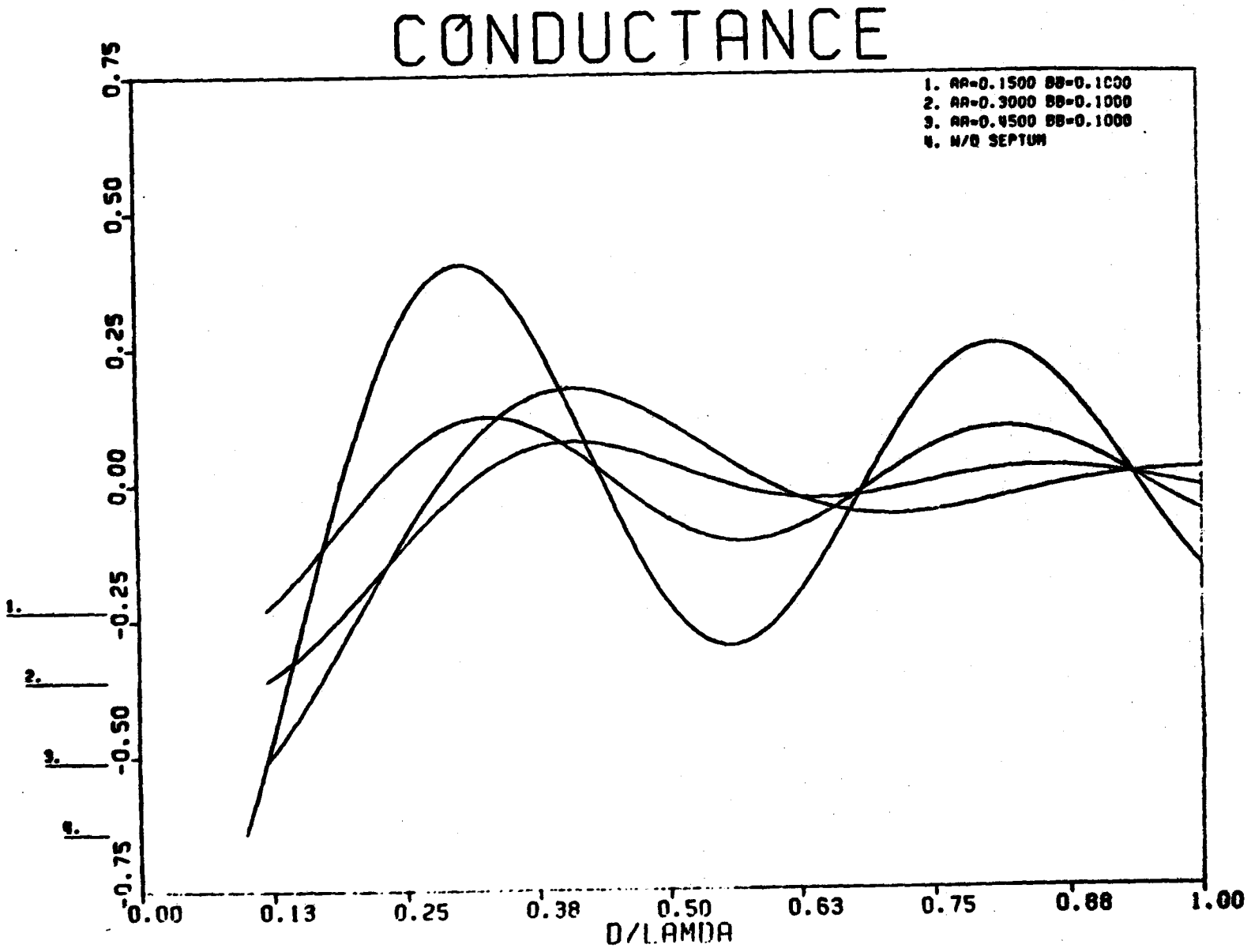
CONDUCTANCE
1. AA=0.1500 BB=0.1000
2. AA=0.3000 BB=0.1000
3. AA=0.4500 BB=0.1000
4. W/O SEPTUM
0.75
0.50
0.25
0.00
-0.25
-0.50
-0.75
1.
2.
3.
4.
0.00
0.13
0.25
0.38
0.50
0.63
0.75
0.88
1.00
D/LAMDA

Figure 22.

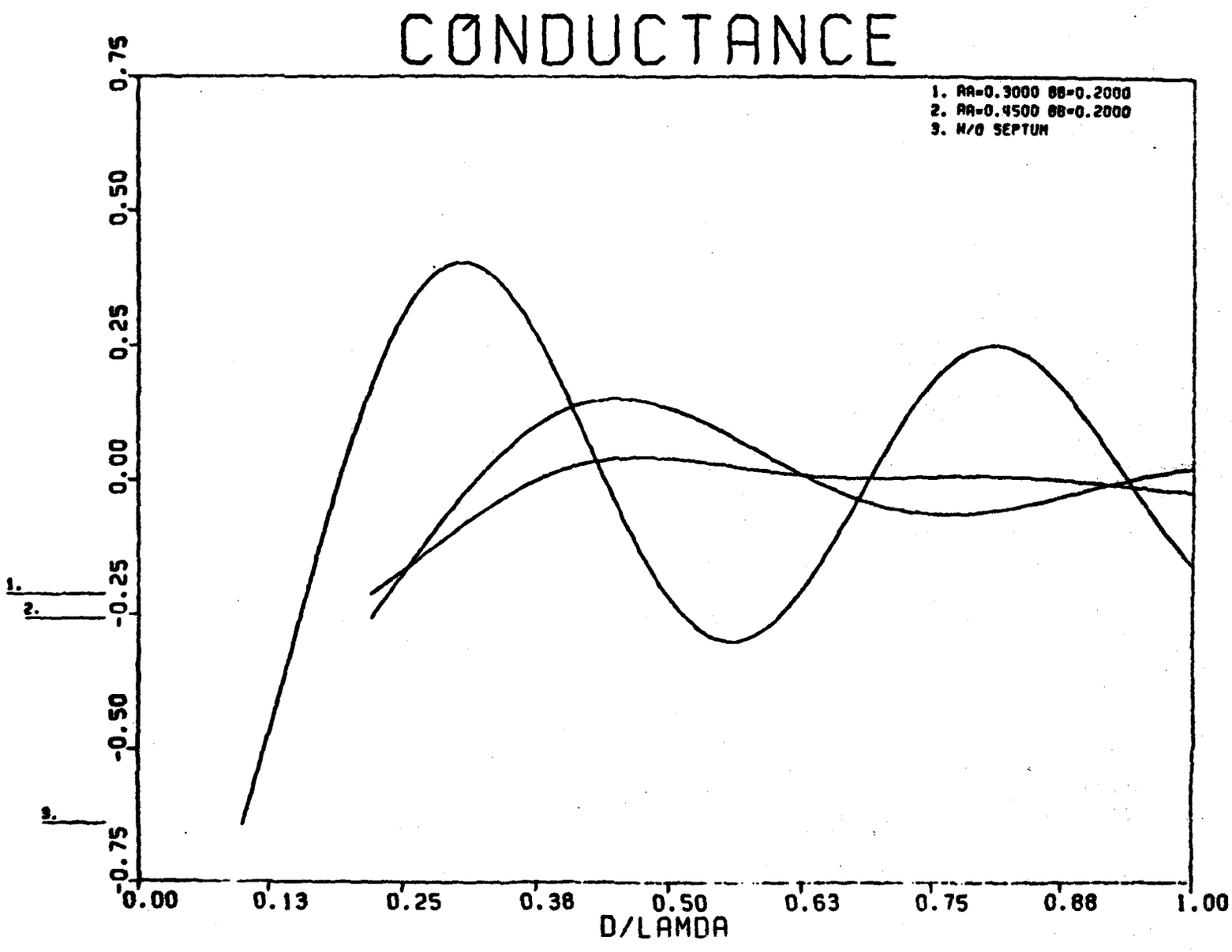
CONDUCTANCE
1. AA=0.3000 BB=0.2000
2. AA=0.4500 BB=0.2000
3. W/O SEPTUM
0.75
0.50
0.25
0.00
-0.25
-0.50
-0.75
1.
2.
3.
0.00
0.13
0.25
0.38
0.50
0.63
0.75
0.88
1.00
D/LAMDA

Figure 23.

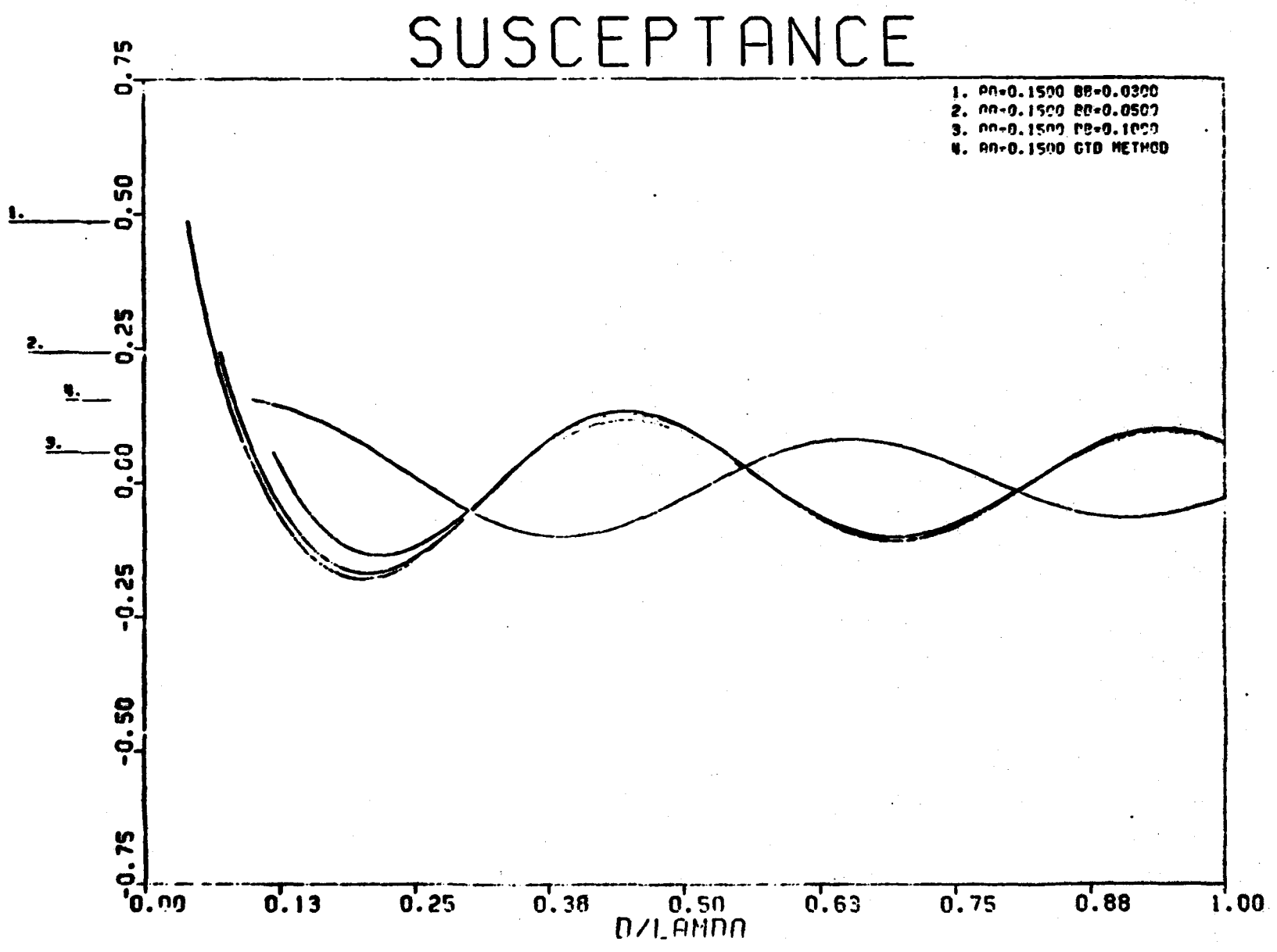
SUSCEPTANCE
1. RA=0.1500 RB=0.0300
2. RA=0.1500 RB=0.0500
3. RA=0.1500 RB=0.1000
4. RA=0.1500 GTD METHOD
0.75
0.50
0.25
0.00
-0.25
-0.50
-0.75
1.
2.
3.
4.
0.00
0.13
0.25
0.38
0.50
0.63
0.75
0.88
1.00
D/LAMDA

Figure 24.

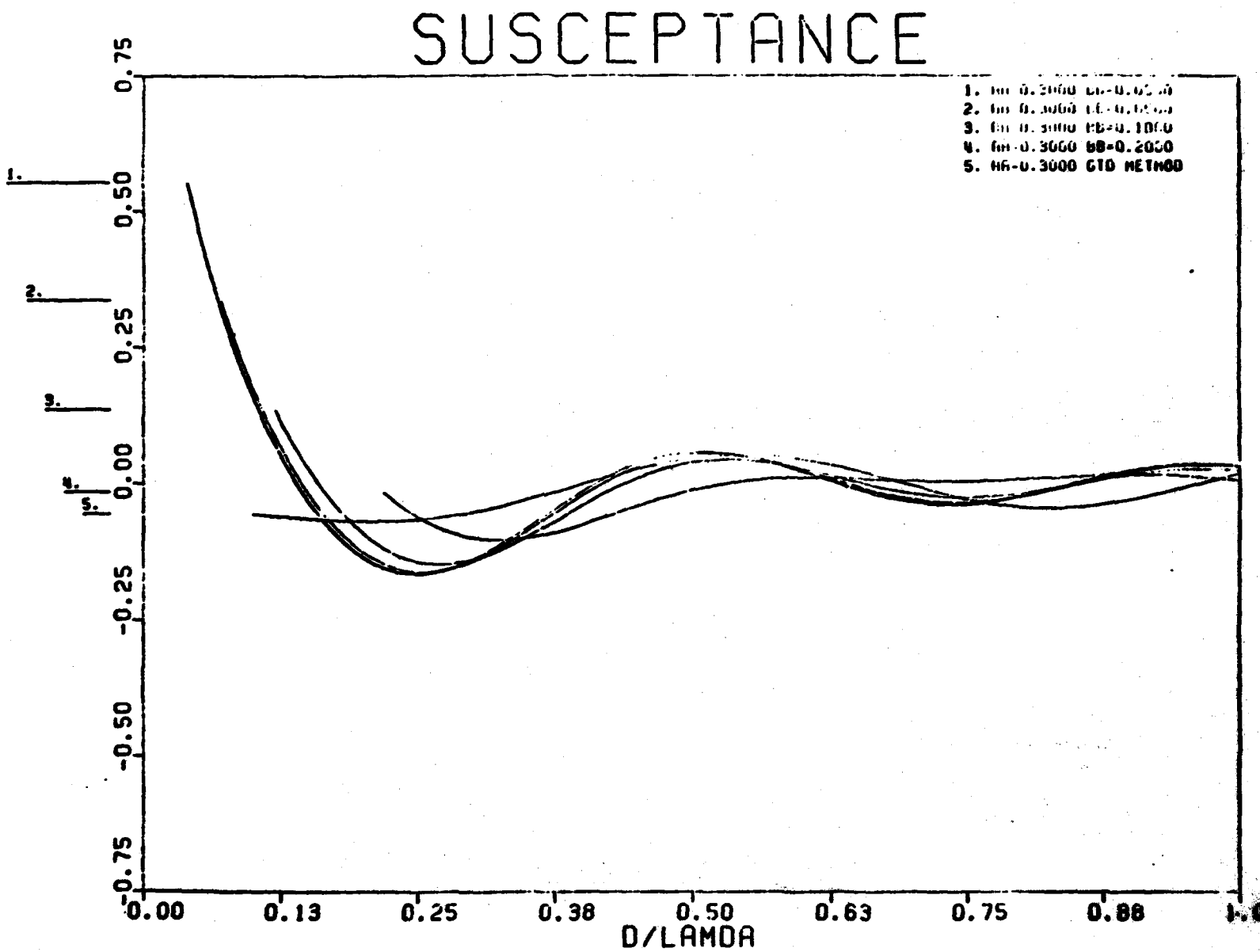
SUSCEPTANCE
1. hm 0.3000 hb=0.0500
2. hm 0.3000 hb=0.1000
3. hm 0.3000 hb=0.1500
4. hm=0.3000 hb=0.2000
5. HA=0.3000 GTD METHOD
0.75
0.50
0.25
0.00
-0.25
-0.50
-0.75
0.00
0.13
0.25
0.38
0.50
0.63
0.75
0.88
1.00
D/LAMDA

Figure 25.

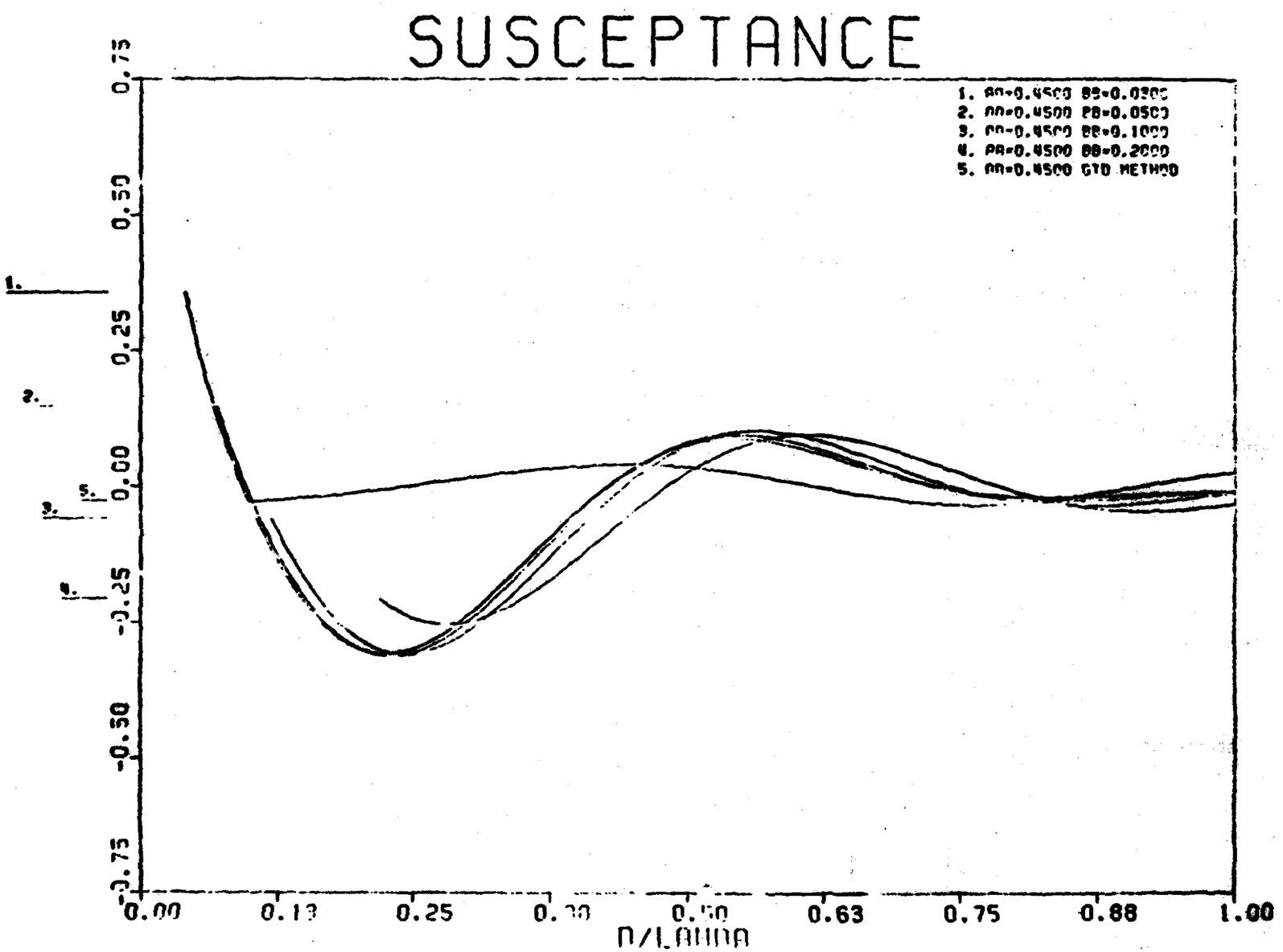
SUSCEPTANCE
1. AA=0.4500 BB=0.0200
2. AA=0.4500 BB=0.0500
3. AA=0.4500 BB=0.1000
4. AA=0.4500 BB=0.2000
5. AA=0.4500 GTD METHOD
0.75
0.50
0.25
0.00
-0.25
-0.50
-0.75
0.00
0.13
0.25
0.38
0.50
0.63
0.75
0.88
1.00
D/LAMDA

Figure 26.

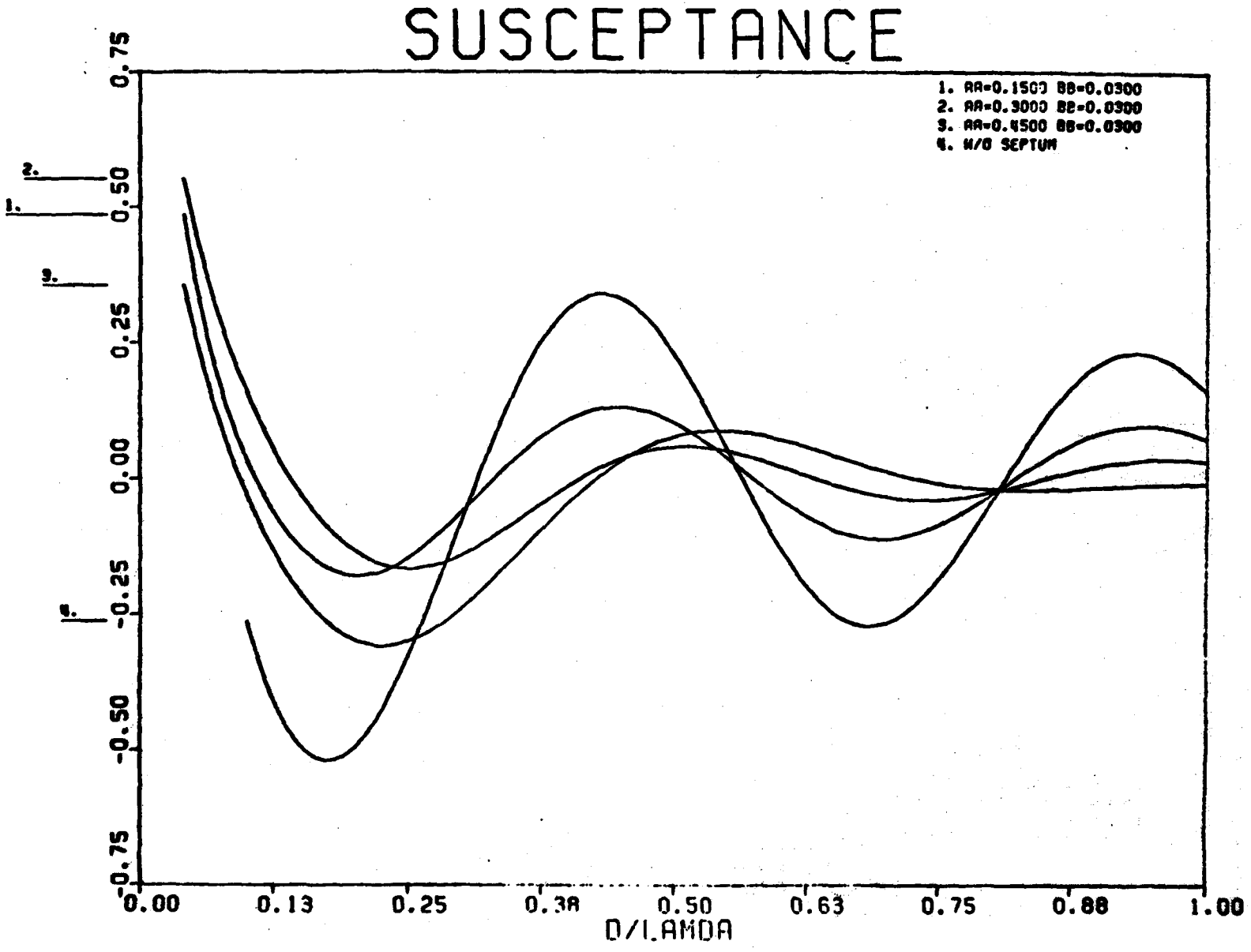
SUSCEPTANCE
1. AA=0.1500 BB=0.0300
2. AA=0.3000 BB=0.0300
3. AA=0.4500 BB=0.0300
4. W/O SEPTUM
0.75
0.50
0.25
0.00
-0.25
-0.50
-0.75
0.00
0.13
0.25
0.38
0.50
0.63
0.75
0.88
1.00
D/LAMDA

Figure 27.

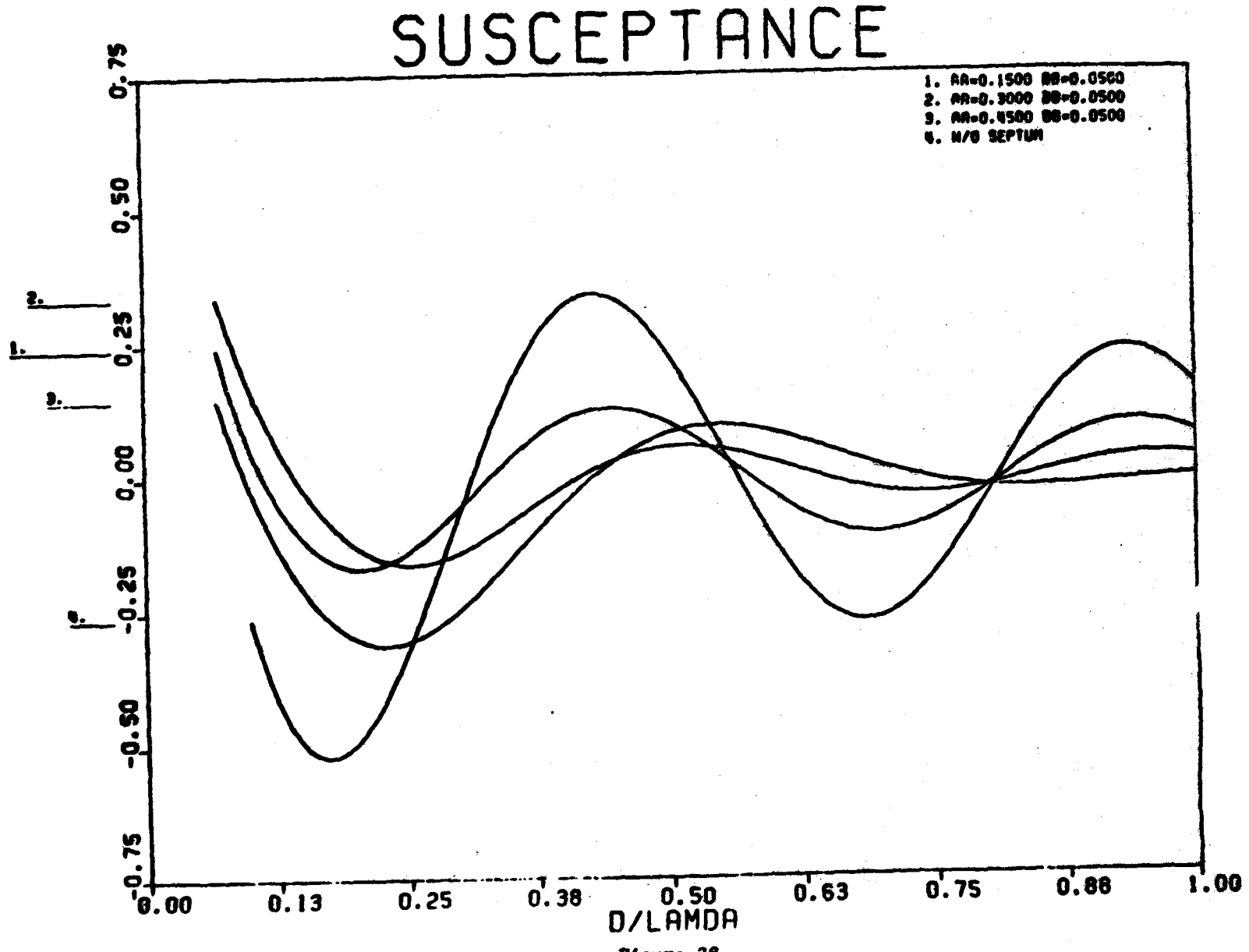
SUSCEPTANCE
1. AA=0.1500 BB=0.0500
2. AA=0.3000 BB=0.0500
3. AA=0.4500 BB=0.0500
4. H/O SEPTUM
0.75
0.50
0.25
0.00
-0.25
-0.50
-0.75
0.00
0.13
0.25
0.38
0.50
0.63
0.75
0.88
1.00
D/LAMDA

Figure 28.

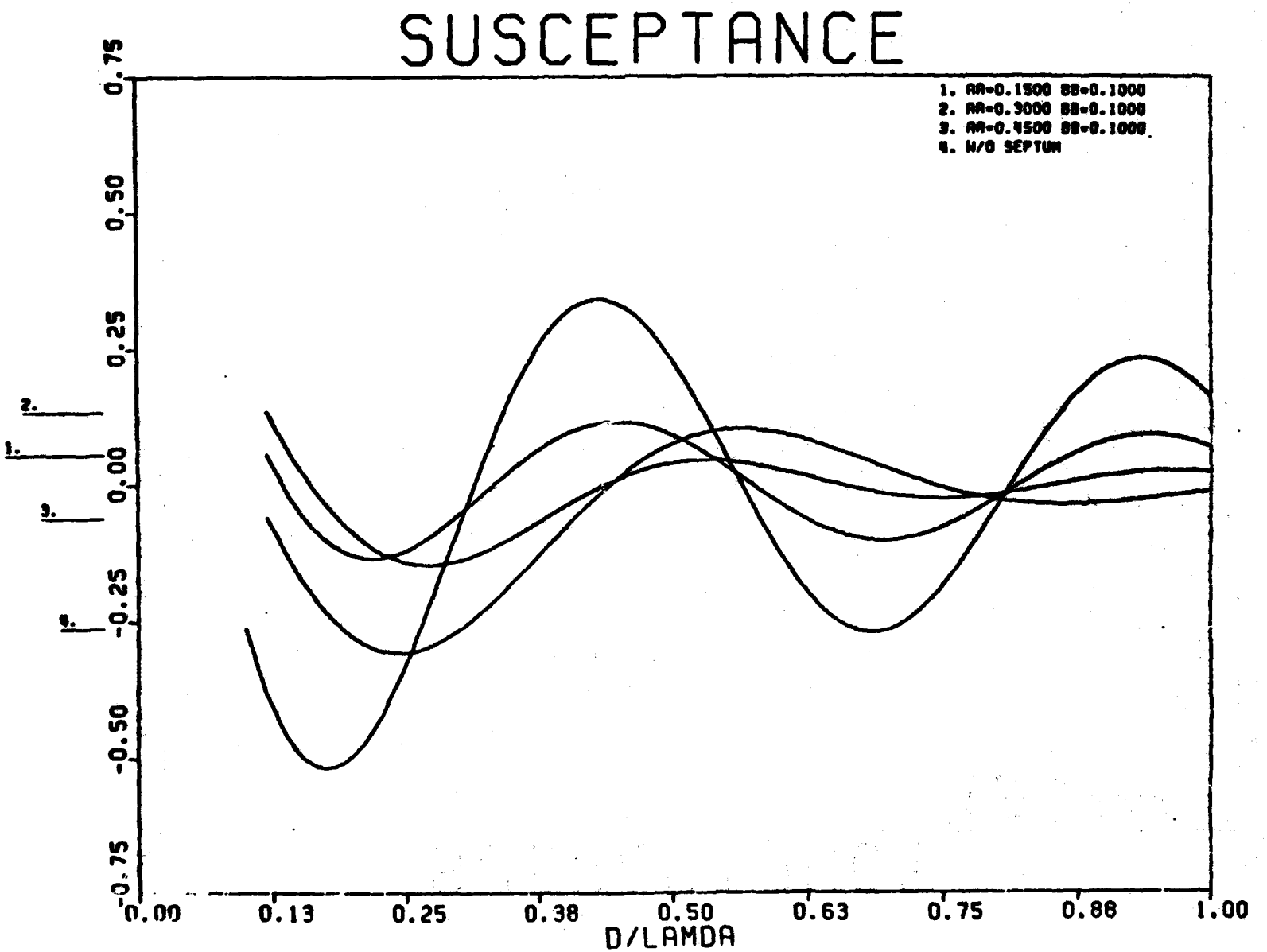
SUSCEPTANCE
1. AA=0.1500 BB=0.1000
2. AA=0.3000 BB=0.1000
3. AA=0.4500 BB=0.1000
4. W/O SEPTUM
0.75
0.50
0.25
0.00
-0.25
-0.50
-0.75
2.
1.
3.
4.
0.00
0.13
0.25
0.38
0.50
0.63
0.75
0.88
1.00
D/LAMDA

Figure 29.

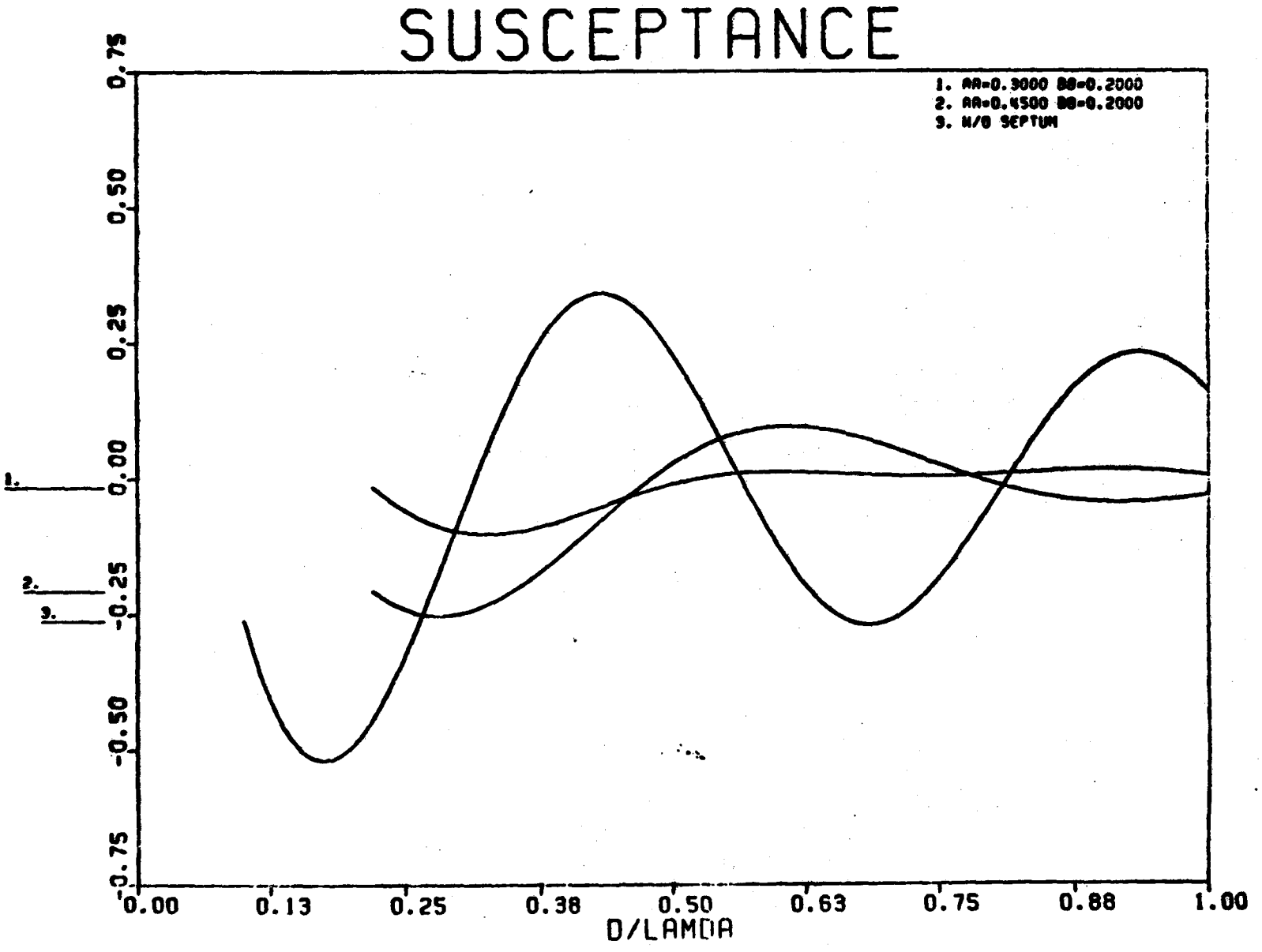
SUSCEPTANCE
1. AA=0.3000 BB=0.2000
2. AA=0.4500 BB=0.2000
3. H/B SEPTUM
0.75
0.50
0.25
0.00
-0.25
-0.50
-0.75
0.00
0.13
0.25
0.38
0.50
0.63
0.75
0.88
1.00
D/LAMDA
1.
2.
3.

Figure 30.

R1 = R2 = 0.3000 a/λ = 0.5000 b/λ = 0.1000

MODAL ANALYSIS OF SCATTERED FIELD

AE MODE

IK	PAE (%)
0	0.663E+00
2	0.488E-01
4	0.143E-02
6	0.309E-03
8	0.795E-04
10	0.167E-04
12	0.339E-05
14	0.682E-06
16	0.138E-06
18	0.280E-07
20	0.572E-08
22	0.324E-10
24	0.195E-10
26	0.840E-11
28	0.266E-11

BO MODE

IK	PBO (%)
1	0.274E+00
3	0.110E-01
5	0.114E-02
7	0.207E-03
9	0.395E-04
11	0.774E-05
13	0.154E-05
15	0.308E-06
17	0.622E-07
19	0.127E-07
21	0.259E-08
23	0.262E-10
25	0.133E-10
27	0.491E-11
29	0.134E-12

FIELDS	REAL	IMAGINARY	MAGNITUDE	PHASE
INCIDENT :	0.2010	-0.0385	0.2046	-10.8412
SCATTERED :	-0.0972	-0.2400	0.2590	67.9425
TOTAL :	0.1037	-0.2785	0.2973	-69.5686

R1 = R2 = 0.5000 a/λ = 0.5000 b/λ = 0.1000

MODAL ANALYSIS OF SCATTERED FIELD

AE MODE

IK	PAE (%)
0	0.650E+00
2	0.655E-01
4	0.688E-03
6	0.254E-04
8	0.138E-05
10	0.722E-07
12	0.384E-08
14	0.208E-09
16	0.114E-10
18	0.639E-12
20	0.361E-13
22	0.566E-16
24	0.950E-17
26	0.114E-17
28	0.101E-18

BO MODE

IK	PBO (%)
1	0.275E+00
3	0.888E-02
5	0.233E-03
7	0.752E-05
9	0.339E-06
11	0.171E-07
13	0.901E-09
15	0.489E-10
17	0.271E-11
19	0.152E-12
21	0.861E-14
23	0.242E-16
25	0.343E-17
27	0.352E-18
29	0.270E-20

FIELDS	REAL	IMAGINARY	MAGNITUDE	PHASE
INCIDENT :	-0.1101	0.1146	0.1589	-46.1259
SCATTERED :	0.2168	-0.0026	0.2168	- 0.6904
TOTAL :	0.1067	0.1119	0.1546	46.3858

R1 = R2 0.3000 a/λ = 0.5000 b/λ = 0.2000

MODAL ANALYSIS OF SCATTERED FIELD

AE MODE

IK	PAE (%)
0	0.508E+00
2	0.512E-01
4	0.103E-01
6	0.479E-02
8	0.189E-02
10	0.753E-03
12	0.305E-03
14	0.125E-03
16	0.522E-04
18	0.219E-04
20	0.931E-05
22	0.398E-05
24	0.243E-07
26	0.403E-07
28	0.491E-07

BO MODE

IK	PBO (%)
1	0.380E+00
3	0.291E-01
5	0.822E-02
7	0.305E-02
9	0.119E-02
11	0.478E-03
13	0.195E-03
15	0.807E-04
17	0.338E-04
19	0.143E-04
21	0.609E-05
23	0.167E-06
25	0.326E-06
27	0.462E-06
29	0.487E-08

FIELDS	REAL	IMAGINARY	MAGNITUDE	PHASE
INCIDENT :	0.2010	-0.0385	0.2046	-10.8412
SCATTERED :	-0.1896	-0.2431	0.3083	52.0410
TOTAL :	0.0114	-0.2815	0.2818	-87.6860

R1 = R2 = 0.5000 a/λ = 0.5000 b/λ = 0.2000

MODAL ANALYSIS OF SCATTERED FIELD

AE MODE

IK	PAE (%)
0	0.517E +00
2	0.633E - 01
4	0.447E - 02
6	0.332E - 03
8	0.264E - 04
10	0.250E - 05
12	0.252E - 06
14	0.265E - 07
16	0.286E - 08
18	0.314E - 09
20	0.350E - 10
22	0.394E - 11
24	0.637E - 14
26	0.280E - 14
28	0.905E - 15

BO MODE

IK	PBO (%)
1	0.391E +00
3	0.225E - 01
5	0.145E - 02
7	0.915E - 04
9	0.805E - 05
11	0.789E - 06
13	0.814E - 07
15	0.867E - 08
17	0.945E - 09
19	0.105E - 09
21	0.117E - 10
23	0.851E - 13
25	0.439E - 13
27	0.165E - 13
29	0.463E - 16

FIELDS	REAL	IMAGINARY	MAGNITUDE	PHASE
INCIDENT :	-0.1101	0.1146	0.1589	-46.1259
SCATTERED :	0.2505	-0.0492	0.2553	-11.1205
TOTAL :	0.1403	0.0653	0.1548	24.9630

R1 = R2 = 0.5000 a/λ = 0.5000 b/λ = 0.4000

MODAL ANALYSIS OF SCATTERED FIELD

AE MODE

IK	PAE (%)
0	0.253E +00
2	0.684E - 01
4	0.815E - 01
6	0.159E - 01
8	0.480E - 02
10	0.173E - 02
12	0.666E - 03
14	0.267E - 03
16	0.110E - 03
18	0.464E - 04
20	0.198E - 04
22	0.853E - 05
24	0.372E - 05
26	0.439E - 07
28	0.148E - 06

BO MODE

IK	PBO (%)
1	0.413E +00
3	0.113E +00
5	0.345E - 01
7	0.841E - 02
9	0.284E - 02
11	0.107E - 02
13	0.420E - 03
15	0.171E - 03
17	0.714E - 04
19	0.302E - 04
21	0.130E - 04
23	0.562E - 05
25	0.213E - 06
27	0.836E - 07
29	0.244E - 07

FIELDS	REAL	IMAGINARY	MAGNITUDE	PHASE
INCIDENT :	-0.1101	0.1146	0.1589	-46.1259
SCATTERED :	0.1750	-0.1702	0.2442	-44.2076
TOTAL :	0.0649	-0.0557	0.0855	-40.6405

R1 = R2 = 0.6000 a/λ = 0.5000 b/λ = 0.4000

MODAL ANALYSIS OF SCATTERED FIELD

AE MODE

IK	PAE (%)
0	0.278E +00
2	0.726E - 01
4	0.640E - 01
6	0.527E - 02
8	0.677E - 03
10	0.118E - 03
12	0.228E - 04
14	0.466E - 95
16	0.991E - 06
18	0.216E - 06
20	0.479E - 07
22	0.108E - 07
24	0.246E - 08
26	0.152E - 10
28	0.269E - 10

BO MODE

IK	PBO (%)
1	0.451E +00
3	0.108E +00
5	0.186E - 01
7	0.177E - 02
9	0.277E - 03
11	0.512E - 04
13	0.102E - 04
15	0.214E - 05
17	0.461E - 06
19	0.102E - 06
21	0.227E - 07
23	0.514E - 08
25	0.102E - 09
27	0.209E - 10
29	0.321E - 11

FIELDS	REAL	IMAGINARY	MAGNITUDE	PHASE
INCIDENT :	-0.1304	-0.0638	0.1451	26.0583
SCATTERED :	0.2118	0.0891	0.2298	22.8073
TOTAL :	0.0815	0.0253	0.0853	17.2710

R1 = R2 = 0.2000 a/λ = 0.7500 b/λ = 0.1000

ATTENTION THE SEPTUM MAY BE TOO BIG FOR ANALYSIS

MODAL ANALYSIS OF SCATTERED FIELD

AE MODE

IK	PAE (%)
0	0.825E+00
2	0.662E-01
4	0.857E-02
6	0.958E-03
8	0.969E-04
10	0.284E-04
12	0.112E-04
14	0.503E-05
16	0.242E-05
18	0.122E-05
20	0.628E-06
22	0.330E-06
24	0.479E-07
26	0.206E-08
28	0.658E-08

BO MODE

IK	PBO (%)
1	0.931E-01
3	0.654E-03
5	0.528E-02
7	0.144E-03
8	0.365E-04
11	0.145E-04
13	0.663E-05
15	0.324E-05
17	0.164E-05
19	0.851E-06
21	0.448E-06
23	0.239E-06
25	0.102E-07
27	0.379E-07
29	0.105E-08

FIELDS	REAL	IMAGINARY	MAGNITUDE	PHASE
INCIDENT :	0.0275	-0.2480	0.2496	-83.6782
SCATTERED :	-0.3809	0.2787	0.4719	-36.1951
TOTAL :	-0.3534	0.0306	0.3547	-4.9567

R1 = R2 = 0.3000 a/λ = 0.7500 b/λ = 0.1000

ATTENTION THE SEPTUM MAY BE TOO BIG FOR ANALYSIS

MODAL ANALYSIS OF SCATTERED FIELD

AE MODE

IK	PAE (%)
0	0.834E+00
2	0.315E-01
4	0.841E-03
6	0.119E-02
8	0.107E-03
10	0.184E-04
12	0.397E-05
14	0.966E-06
16	0.254E-06
18	0.708E-07
20	0.205E-07
22	0.609E-08
24	0.504E-09
26	0.124E-10
28	0.229E-10

BO MODE

IK	PBO (%)
1	0.126E+00
3	0.267E-02
5	0.380E-02
7	0.186E-03
9	0.315E-04
11	0.696E-05
13	0.173E-05
15	0.459E-06
17	0.128E-06
19	0.370E-07
21	0.110E-07
23	0.332E-08
25	0.813E-10
27	0.174E-09
29	0.280E-11

FIELDS		REAL	IMAGINARY	MAGNITUDE	PHASE
INCIDENT	:	0.2010	-0.0385	0.2046	-10.8412
SCATTERED	:	-0.4071	0.0503	0.4102	-7.0467
TOTAL	:	-0.2061	0.0118	0.2065	-3.3858

R1 = R2 = 0.4000 a/λ = 0.7500 b/λ = 0.1000

ATTENTION THE SEPTUM MAY BE TOO BIG FOR ANALYSIS

MODAL ANALYSIS OF SCATTERED FIELD

AE MODE

IK	PAE (%)
0	0.794E+00
2	0.147E-01
4	0.101E-01
6	0.256E-02
8	0.110E-03
10	0.109E-04
12	0.140E-05
14	0.208E-06
16	0.335E-07
18	0.573E-08
20	0.102E-08
22	0.187E-09
24	0.951E-11
26	0.145E-12
28	0.164E-12

BO MODE

IK	PBO (%)
1	0.156E+00
3	0.739E-02
5	0.149E-01
7	0.265E-03
9	0.243E-04
11	0.317E-05
13	0.475E-06
15	0.773E-07
17	0.132E-07
19	0.235E-08
21	0.429E-09
23	0.800E-10
25	0.121E-11
27	0.159E-11
29	0.157E-13

FIELDS	REAL	IMAGINARY	MAGNITUDE	PHASE
INCIDENT :	0.0844	0.1562	0.1775	61.6015
SCATTERED :	-0.2960	-0.1520	0.3327	27.1775
TOTAL :	-0.2116	0.0042	0.2116	-1.1338

R1 = R2 = 0.3000 a/λ = 0.7500 b/λ = 0.2000

ATTENTION THE SEPTUM MAY BE TOO BIG FOR ANALYSIS

MODAL ANALYSIS OF SCATTERED FIELD

AE MODE

IK	PAE (%)
0	0.798E+00
2	0.276E-01
4	0.119E-02
6	0.839E-03
8	0.356E-03
10	0.163E-03
12	0.796E-03
14	0.406E-04
16	0.213E-04
18	0.115E-04
20	0.631E-05
22	0.351E-05
24	0.198E-05
26	0.104E-06
28	0.594E-07

BO MODE

IK	PBO (%)
1	0.165E+00
3	0.444E-02
5	0.103E-02
7	0.480E-03
9	0.227E-03
11	0.111E-03
13	0.561E-04
15	0.292E-04
17	0.156E-04
19	0.849E-05
21	0.470E-05
23	0.263E-05
25	0.387E-07
27	0.257E-06
29	0.128E-07

FIELDS		REAL	IMAGINARY	MAGNITUDE	PHASE
INCIDENT	:	0.2010	-0.0385	0.2046	-10.8412
SCATTERED	:	-0.4461	0.1310	0.4649	-16.3638
TOTAL	:	-0.2451	0.0925	0.2620	-20.6752

R1 = R2 = 0.4000 a/λ = 0.7500 b/λ = 0.2000

ATTENTION THE SEPTUM MAY BE TOO BIG FOR ANALYSIS

MODAL ANALYSIS OF SCATTERED FIELD

AE MODE

IK	PAE (%)
0	0.760E+00
2	0.141E-01
4	0.516E-02
6	0.115E-02
8	0.244E-03
10	0.637E-04
12	0.184E-04
14	0.561E-05
16	0.178E-05
18	0.580E-06
20	0.193E-06
22	0.651E-07
24	0.223E-07
26	0.708E-09
28	0.247E-09

BO MODE

IK	PBO (%)
1	0.206E+00
3	0.103E-01
5	0.228E-02
7	0.450E-03
9	0.117E-03
11	0.332E-04
13	0.100E-04
15	0.314E-05
17	0.101E-05
19	0.333E-06
21	0.112E-06
23	0.380E-07
25	0.339E-09
27	0.137E-08
29	0.414E-10

FIELDS	REAL	IMAGINARY	MAGNITUDE	PHASE
INCIDENT :	0.0844	0.1562	0.1775	61.6015
SCATTERED :	-0.3328	-0.1416	0.3616	23.0524
TOTAL :	-0.2483	0.0146	0.2488	-3.3546

R1 = R2 = 0.4000 a/λ = 0.7500 b/λ = 0.3000

ATTENTION THE SEPTUM MAY BE TOO BIG FOR ANALYSIS

MODAL ANALYSIS OF SCATTERED FIELD

AE MODE

IK	PAE (%)
0	0.734E+00
2	0.126E-01
4	0.760E-02
6	0.132E-02
8	0.184E-03
10	0.148E-04
12	0.415E-04
14	0.341E-04
16	0.230E-04
18	0.144E-04
20	0.872E-05
22	0.518E-05
24	0.304E-05
26	0.695E-07
28	0.605E-07

BO MODE

IK	PBO (%)
1	0.223E+00
3	0.169E-01
5	0.339E-02
7	0.489E-03
9	0.422E-04
11	0.367E-04
13	0.392E-04
15	0.284E-04
17	0.183E-04
19	0.113E-04
21	0.673E-05
23	0.397E-05
25	0.232E-05
27	0.213E-06
29	0.159E-06

FIELDS	REAL	IMAGINARY	MAGNITUDE	PHASE
INCIDENT :	0.0844	0.1562	0.1775	61.6015
SCATTERED :	-0.3889	-0.0551	0.3928	8.0666
TOTAL :	-0.3045	0.1010	0.3208	-18.3606

R1 = R2 = 0.5000 a/λ = 0.7500 b/λ = 0.3000

ATTENTION THE SEPTUM MAY BE TOO BIG FOR ANALYSIS

MODAL ANALYSIS OF SCATTERED FIELD

AE MODE

IK	PAE (%)
0	0.682E+00
2	0.191E-01
4	0.108E-01
6	0.948E-03
8	0.660E-04
10	0.301E-05
12	0.497E-05
14	0.244E-05
16	0.994E-06
18	0.377E-06
20	0.139E-06
22	0.502E-07
24	0.180E-07
26	0.251E-09
28	0.134E-09

BO MODE

IK	PBO (%)
1	0.259E+00
3	0.241E-01
5	0.356E-02
7	0.242E-03
9	0.571E-05
11	0.571E-05
13	0.362E-05
15	0.158E-05
17	0.616E-06
19	0.230E-06
21	0.836E-07
23	0.301E-07
25	0.107E-07
27	0.603E-09
29	0.276E-09

FIELDS		REAL	IMAGINARY	MAGNITUDE	PHASE
INCIDENT	:	-0.1101	0.1146	0.1589	-46.1259
SCATTERED	:	-0.1672	-0.2162	0.2733	52.2907
TOTAL	:	-0.2773	-0.1017	0.2954	20.1365

[illegible] = 0.[illegible] a/λ = 1.[illegible] b/λ = 0.1000

[illegible]

[illegible]

AE MODE

IK	FNE ($)
1	0.[illegible]E+00
2	0.[illegible]E-01
3	0.[illegible]E-01
4	0.[illegible]E-01
5	0.[illegible]E-02
6	0.[illegible]E-02
7	0.[illegible]E-02
8	0.[illegible]E-03
9	0.[illegible]E-03
10	0.[illegible]E-03
11	0.[illegible]E-03
12	0.[illegible]E-04
13	0.[illegible]E-04
14	0.[illegible]E-04
15	0.[illegible]E-05

BO MODE

IK	FBO ($)
1	0.[illegible]E-01
2	0.[illegible]E+00
3	0.[illegible]E-01
4	0.[illegible]E-02
5	0.[illegible]E-02
6	0.[illegible]E-02
7	0.[illegible]E-03
8	0.[illegible]E-03
9	0.[illegible]E-03
10	0.[illegible]E-03
11	0.[illegible]E-03
12	0.[illegible]E-04
13	0.[illegible]E-04
14	0.[illegible]E-05
15	0.[illegible]E-06

FIELDS	REAL	IMAGINARY	MAGNITUDE	PHASE
INCIDENT :	0.0275	-0.2480	0.[illegible]	-83.6782
SCATTERED :	-0.1579	-0.1224	0.[illegible]	37.7783
TOTAL :	-0.1304	-0.3704	0.3927	70.6055

R1 = R2 = 0.3000 a/λ = 1.0000 b/λ = 0.1000

ATTENTION THE SEPTUM MAY BE TOO BIG FOR ANALYSIS

MODAL ANALYSIS OF SCATTERED FIELD

AE MODE

IK	PAE (%)
0	0.733E+00
2	0.465E-01
4	0.207E-01
6	0.419E-02
8	0.983E-03
10	0.304E-03
12	0.106E-03
14	0.391E-04
16	0.150E-04
18	0.593E-05
20	0.239E-05
22	0.974E-06
24	0.402E-06
26	0.168E-06
28	0.103E-07

BO MODE

IK	PBO (%)
1	0.825E-01
3	0.939E-01
5	0.158E-01
7	0.168E-02
9	0.475E-03
11	0.161E-03
13	0.596E-04
15	0.230E-04
17	0.909E-05
19	0.366E-05
21	0.150E-05
23	0.618E-06
25	0.258E-06
27	0.395E-07
29	0.247E-08

FIELDS	REAL	IMAGINARY	MAGNITUDE	PHASE
INCIDENT :	0.2010	-0.0385	0.2046	-10.8412
SCATTERED :	-0.1086	-0.1923	0.2209	60.5402
TOTAL :	0.0924	-0.2308	0.2486	-68.1862

R1 = R2 = 0.3000 a/λ = 1.0000 b/λ = 0.2000

ATTENTION THE SEPTUM MAY BE TOO BIG FOR ANALYSIS

MODAL ANALYSIS OF SCATTERED FIELD

AE MODE

IK	PAE (%)
0	0.651E +00
2	0.499E - 01
4	0.183E - 01
6	0.158E - 01
8	0.470E - 02
10	0.205E - 02
13	0.103E - 02
14	0.553E - 03
16	0.311E - 03
18	0.180E - 03
20	0.106E - 03
22	0.638E - 04
24	0.387E - 04
26	0.238E - 04
28	0.306E - 05

BO MODE

IK	PBO (%)
1	0.841E - 01
3	0.933E - 01
5	0.641E - 01
7	0.823E - 02
9	0.306E - 02
11	0.144E - 02
13	0.749E - 03
15	0.413E - 03
17	0.236E - 03
19	0.138E - 03
21	0.822E - 04
23	0.496E - 04
25	0.303E - 04
27	0.823E - 05
29	0.106E - 05

FIELDS		REAL	IMAGINARY	MAGNITUDE	PHASE
INCIDENT	:	0.2010	-0.0385	0.2046	-10.8412
SCATTERED	:	-0.1602	-0.1629	0.2285	45.4837
TOTAL	:	0.0408	-0.2014	0.2055	-78.5515

R1 = R2 = 0.4000 a/λ = 1.0000 b/λ = 0.2000

ATTENTION THE SEPTUM MAY BE TOO BIG FOR ANALYSIS

MODAL ANALYSIS OF SCATTERED FIELD

AE MODE

IK	PAE (%)
0	0.690E+00
2	0.656E-01
4	0.357E-01
6	0.543E-02
8	0.808E-03
10	0.211E-03
12	0.678E-04
14	0.240E-04
16	0.897E-05
18	0.348E-05
20	0.138E-05
22	0.561E-06
24	0.230E-06
26	0.957E-07
28	0.836E-08

BO MODE

IK	PBO (%)
1	0.113E+00
3	0.573E-01
5	0.301E-01
7	0.194E-02
9	0.402E-03
11	0.118E-03
13	0.400E-04
15	0.146E-04
17	0.557E-05
19	0.219E-05
21	0.879E-06
23	0.359E-06
25	0.148E-06
27	0.273E-07
29	0.239E-08

FIELDS	REAL	IMAGINARY	MAGNITUDE	PHASE
INCIDENT :	0.0844	0.1562	0.1775	61.6015
SCATTERED :	-0.0353	-0.2229	0.2257	80.9904
TOTAL :	0.0491	0.0668	0.0829	-53.6870

R1 = R2 = 0.4000 a/λ = 1.0000 b/λ = 0.3000

ATTENTION THE SEPTUM MAY BE TOO BIG FOR ANALYSIS

MODAL ANALYSIS OF SCATTERED FIELD

AE MODE

IK	PAE (%)
0	0.607E+00
2	0.749E-01
4	0.422E-01
6	0.614E-01
8	0.485E-02
10	0.146E-02
12	0.613E-03
14	0.297E-03
16	0.156E-03
18	0.856E-04
20	0.487E-04
22	0.284E-04
24	0.169E-04
26	0.102E-04
28	0.137E-05

BO MODE

IK	PBO (%)
1	0.867E-01
3	0.350E-01
5	0.679E-01
7	0.127E-01
9	0.251E-02
11	0.926E-03
13	0.422E-03
15	0.213E-03
17	0.115E-03
19	0.643E-04
21	0.371E-04
23	0.218E-04
25	0.131E-04
27	0.792E-05
29	0.552E-06

FIELDS		REAL	IMAGINARY	MAGNITUDE	PHASE
INCIDENT	:	0.0844	0.1562	0.1775	61.6015
SCATTERED	:	-0.1128	-0.1552	0.1918	53.9726
TOTAL	:	-0.0284	0.0010	0.0284	-2.0325